(non-specific) IgG2a was used instead of dIgGs, the binding of both protein A and ZZ-BNCs to the cIgG–Ag complexes was not observed. A similar result was obtained in the sandwich ELISA using chicken IgY as Ag and anti-chicken IgY rabbit polyclonal IgG as cIgGs and dIgGs (data not shown). These results corroborated that ZZ-BNCs could recognize dIgGs specifically, even if the same IgG was used as the cIgG. The mechanism underlying the specific recognition of dIgGs by ZZ-BNCs will be discussed later. The sensitivity of the sandwich ELISA is defined by the limit of detection (LOD; mean ± 3SD) and the limit of quantitation (LOQ; mean ± 10SD)[21] at the lowest end of the quantifiable concentration range of human desmin and chicken IgY ($n = 20$). The LOD and LOQ of sandwich ELISAs for human desmin were 125 ng mL^{-1} (coefficient of variation [CV] = 8.0%) and 250 ng mL^{-1} (CV = 6.5%), respectively, and those for chicken IgY were 8 ng mL^{-1} (CV = 3.0%) and 16 ng mL^{-1} (CV = 3.9%), respectively. These values indicated that both sandwich ELISAs were reliable and useful for the detection of low levels of Ags.

Effect of ZZ-BNCs on the sandwich immunoassay using QCM

The ability of ZZ-BNCs to specifically recognize dIgGs in a sandwich ELISA led us to examine whether ZZ-BNCs can distinguish dIgGs from cIgGs in immunoassays. In QCM, the gold surface of the sensor chip was brought into contact with anti-human desmin mouse monoclonal IgG2a (as cIgGs), blocked with 0.2% Block Ace (a mixture of 2% casein and 0.1% Tween-20), allowed to react with the same IgG (this time as dIgGs), and then mixed with ZZ-BNCs. As shown in Fig. 2A, neither dIgGs nor ZZ-BNCs resulted in a frequency change (2 ± 4 ng cm^{-2} and 4 ± 2 ng cm^{-2}, respectively), indicating that cIgGs on a solid phase could not interact with dIgGs and ZZ-BNCs. Under similar conditions, ZZ-BNCs could not interact with various cIgGs on a solid phase, *e.g.* anti-chicken IgY rabbit polyclonal IgG (2 ng cm^{-2} [$n = 2$]) and anti-β-tubulin mouse monoclonal IgG2b (4 ng cm^{-2} [$n = 1$]). In the presence of human desmin (Ag, 1 μg mL^{-1}), small amounts of dIgGs were immobilized onto a solid phase (6 ± 2 ng cm^{-2}), and then ZZ-BNCs were efficiently bound to dIgGs on a solid phase in a human desmin-dependent manner (329 ± 12 ng cm^{-2}; Fig. 2B). According to the increase of the amount of human desmin, the binding of dIgGs (indicating specific binding) and ZZ-BNCs (indicating minimal non-specific binding) to the cIgG–Ag complexes on the solid phase increased marginally, while the amount of dIgG–ZZ-BNC complexes (indicating specific binding of both dIgGs and ZZ-BNCs) bound to the cIgG–Ag complexes

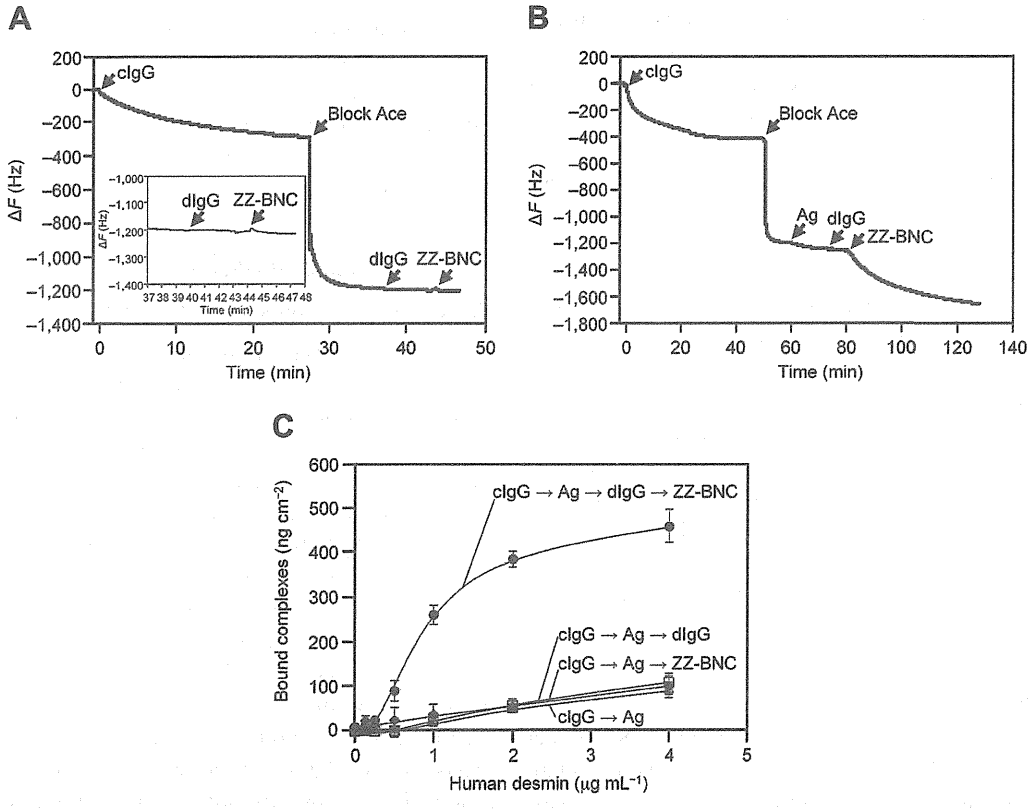

Fig. 2 Detection of human desmin by sandwich immunoassays in QCM using an anti-human desmin mouse monoclonal IgG2a as cIgGs and dIgGs. (A) Without human desmin. (B) With human desmin (1 μg mL^{-1}). The frequency changes (Δ*F*) upon successive injections of cIgGs (2 μg mL^{-1}), Block Ace (blocking reagent, 2 mg mL^{-1}), Ags (human desmin, 1 μg mL^{-1}), detection immunoglobulin Gs (dIgGs, 2 μg mL^{-1}), and ZZ-BNCs (2 μg protein mL^{-1}) were recorded (arrows). The inset is a magnified image of the QCM profile for the binding of dIgGs and ZZ-BNCs. (C) Relationships between the concentration of human desmin (μg mL^{-1}) and the frequency change (ng cm^{-2}; 1 Hz was equivalent to 0.6 ng cm^{-2}) in the detection by cIgG–Ag (open triangles), cIgG–Ag–dIgG (open squares), cIgG–Ag–ZZ-BNC (closed diamonds), and cIgG–Ag–dIgG–ZZ-BNCs (closed circles). The *Y*-axis indicates the sum of bound molecules added in steps after blocking with Block Ace. Results are presented as means ± SD ($n = 3$).

increased significantly (Fig. 2C). When the mouse isotype control (non-specific) IgG2a was used instead of dIgGs, the binding of ZZ-BNCs to the cIgG–Ag complexes was not observed. These results confirmed that ZZ-BNCs could form specific immunocomplexes with cIgG–Ag–dIgG complexes on a solid phase in sandwich immunoassays, using ELISA and QCM, by discriminating dIgGs from cIgGs.

Surface analysis of the immunosensor chip by AFM

We next analyzed the topographical images (500 × 500 nm) of immunocomplexes on a gold substrate (equivalent to the surface of a sensor chip) by AFM. The weight change of the gold substrate was also measured by QCM (Fig. 3, Table 1, and ESI Fig. 1†). The height of the bare gold substrate was 1.07 ± 0.30 nm (ESI Fig. 1A†). After modification with the blocking reagent (0.2% Block Ace), the height and weight of gold substrates were increased to 2.36 ± 0.08 nm and by 451.8 ± 33.0 ng cm^{-2}, respectively. The addition of ZZ-BNCs (Fig. 1A; 32.4 ± 4.0 nm (n = 50) in diameter)[16] was found not to affect the height and weight of gold substrates (ESI Fig. 1C†), indicating that Block Ace completely reduced the nonspecific interaction of ZZ-BNCs. When the Ag (human desmin)-coated gold substrate was blocked with Block Ace, the addition of ZZ-BNCs did not affect the height and weight of gold substrates (ESI Fig. 1F†), but the use of dIgGs (anti-human desmin mouse monoclonal IgG2a)

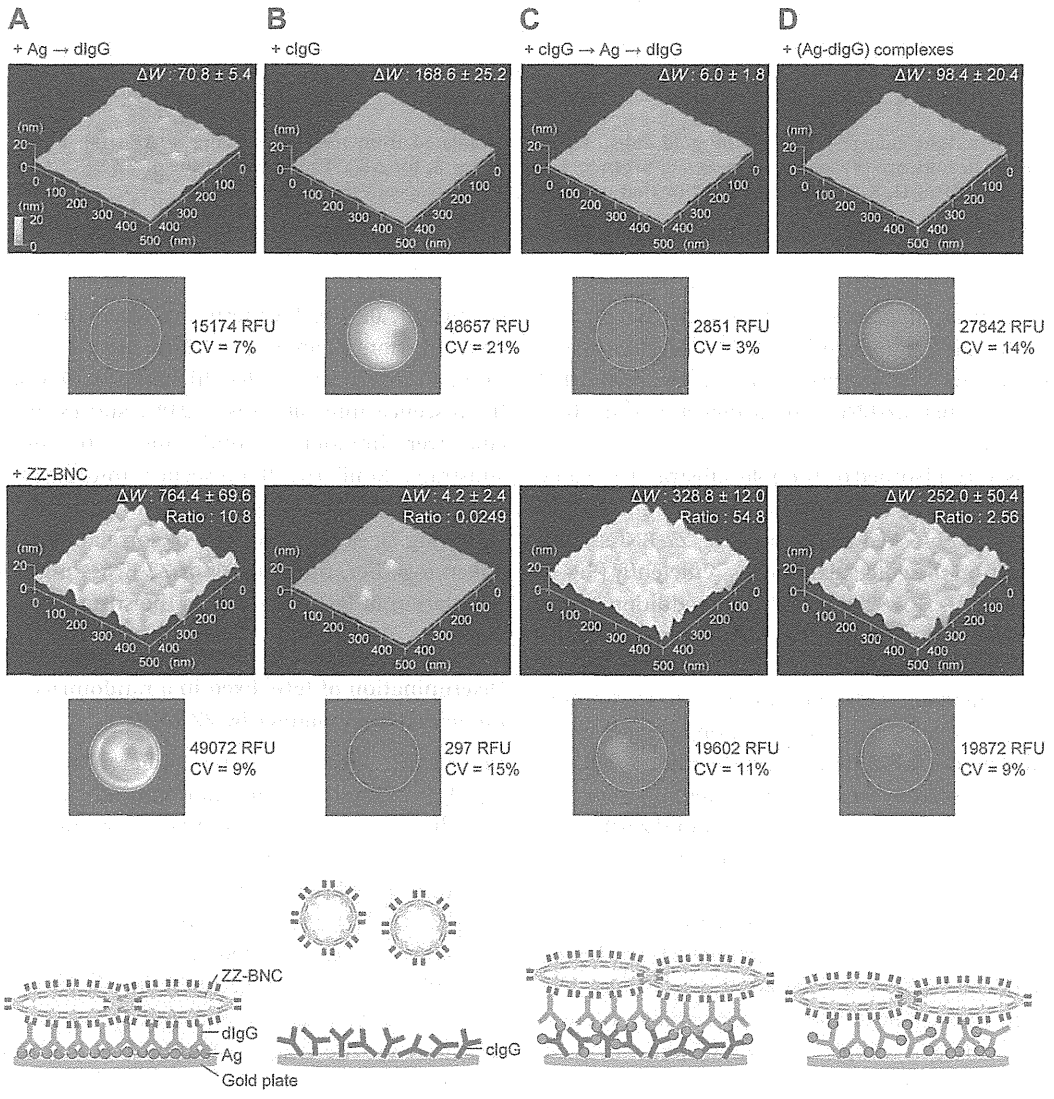

Fig. 3 Atomic force microscopy (AFM) and fluorescence images of gold substrates on QCM sensor chips. 1st and 3rd lines, AFM images (500 × 500 nm) of immunocomplexes with/without ZZ-BNCs. The changes of weight (ΔW) and the ratio of bound ZZ-BNCs to bound c/dIgGs are shown in upper right. 2nd and 4th lines, fluorescence images (diameter, 2.5 mm; area, 4.9 mm^2; 540 pixels) of immunocomplexes with/without ZZ-BNCs. Fluorescence intensities (RFU, relative fluorescence units) and CV (n = 540) are shown in right margins. Bottom line, schema of immunocomplexes immobilized on the gold substrates with ZZ-BNCs. Row A, the bare gold substrate was modified with antigens (Ags; human desmin), Block Ace, dIgGs (anti-human desmin mouse monoclonal IgG2a), and ZZ-BNCs; row B, cIgGs (anti-human desmin mouse monoclonal IgG2a), Block Ace, and ZZ-BNCs; row C, cIgGs, Block Ace, Ags, dIgGs, and ZZ-BNCs; and row D, (Ag–dIgG) complexes, Block Ace, and ZZ-BNCs. The height, diameter and oblateness of ZZ-BNCs (n = 6) in each row were 8.13 ± 1.52 nm, 60.62 ± 5.13 nm and 7.61 ± 1.05 (for row A); 8.61 ± 1.02 nm, 52.72 ± 4.53 nm and 6.15 ± 0.28 (for row B); 7.83 ± 1.18 nm, 54.30 ± 5.07 nm and 7.03 ± 0.95 (for row C); 9.90 ± 1.02 nm, 54.31 ± 1.10 nm and 5.53 ± 0.56 (for row D), respectively.

Table 1 Changes in height and weight of the substrates[a]

	ESI Fig. 1† panel numbers	H (nm)	ΔW (ng cm^{-2})	ZZ-BNC–IgG (w/w)
Bare	A	1.07 ± 0.30		
+Block	B	2.36 ± 0.08	451.8 ± 33.0	
+ZZ-BNC	C	2.27 ± 0.15	1.2 ± 1.2	
+Ag	D	1.28 ± 0.10	375.6 ± 6.0	
+Block	E	3.44 ± 0.55	331.8 ± 40.2	
+ZZ-BNC	F	3.70 ± 0.72	5.4 ± 3.0	
+dIgG	G	4.96 ± 0.54	70.8 ± 5.4	
+ZZ-BNC	H (Fig. 3A)	10.79 ± 1.58	764.4 ± 69.6	10.8
+cIgG	I	2.28 ± 0.48	168.6 ± 25.2	
+Block	J	2.81 ± 0.24	477.6 ± 65.4	
+ZZ-BNC	K (Fig. 3B)	3.18 ± 0.15	4.2 ± 2.4	0.0249
+Ag	L	3.56 ± 0.31	52.2 ± 13.2	
+dIgG	M	3.09 ± 0.49	6.0 ± 1.8	
+ZZ-BNC	N (Fig. 3C)	9.02 ± 1.62	328.8 ± 12.0	54.8
+Ag–dIgG complex (as a dIgG moiety, 60.5% of the total weight)	O	2.84 ± 0.39	162.6 ± 33.6 (98.4 ± 20.4)	
+Block	P	2.66 ± 0.41	451.8 ± 60.0	
+ZZ-BNC	Q (Fig. 3D)	8.42 ± 0.71	252.0 ± 50.4	2.56

[a] H, height (nm). The weight changes (ΔW) in the gold substrate were calculated from frequency changes (ΔF [Hz]; 1 Hz was equivalent to 0.6 ng cm^{-2}) in QCM. Results are presented as means ± SD (n = 5, for H; n = 3, for ΔW). The weight ratios of ZZ-BNC to IgG in H, K, N, and Q were calculated from ΔW of H, K, N, and Q, divided by that of G, I, M, and O, respectively.

followed by the addition of ZZ-BNCs increased the height and weight of gold substrates significantly to 10.79 ± 1.58 nm and by 764.4 ± 69.6 ng cm^{-2}, respectively (Fig. 3, row A and ESI Fig. 1H†), indicating that ZZ-BNCs could detect the Ag–dIgG complexes on a solid phase.

When the cIgGs were adsorbed on the gold substrate (the same antibodies used as dIgGs, *viz.*, anti-human desmin mouse monoclonal IgG2a) and blocked with Block Ace, ZZ-BNCs interacted with the cIgGs on the gold substrate less efficiently (Fig. 3, row B and ESI Fig. 1K†). However, after further addition of Ags and dIgGs, the height and weight of gold substrates were significantly increased by the addition of ZZ-BNCs to 9.02 ± 1.62 nm and by 328.8 ± 12.0 ng cm^{-2}, respectively (Fig. 3, row C and ESI Fig. 1N†). When the mouse isotype control (non-specific) IgG2a was used instead of dIgGs, the binding of ZZ-BNCs to the cIgG–Ag complexes was not observed. Based on the increments in the weight of the gold substrates, the ratio (54.8) of bound ZZ-BNCs to bound dIgGs (Fig. 3, row C) was about 2200 times the ratio (0.0249) of bound ZZ-BNCs to bound cIgGs (Fig. 3, row B). Moreover, the ratio (10.8) of bound ZZ-BNCs to bound dIgGs (Fig. 3, row A) was about 430 times the ratio (0.0249) of bound ZZ-BNCs to bound cIgGs (Fig. 3, row B). These results also strongly suggested that ZZ-BNCs could preferentially bind to Ag–dIgG rather than to cIgGs complexes on a solid phase in QCM, even if the same IgGs were used as cIgGs and dIgGs.

Next, we investigated the surface density of IgGs and ZZ-BNCs on each gold substrate of the QCM sensor chip by using Cy3-labeled and Cy5-labeled forms, respectively. Based on the fluorescence intensity of each gold substrate (Fig. 3, 2nd line), different amounts of Cy3-labeld IgGs were immobilized onto the gold substrate. The values were well correlated with the IgG amounts determined by QCM (Fig. 3, 1st line) (correlation coefficient, 0.979). Furthermore, when the whole area of the gold substrate (diameter, 2.5 mm; area, 4.9 mm^2) was divided into 540 pixels, the CV (coefficient of variation) value of each fluorescence intensity was 3–21%, suggesting that IgG molecules were immobilized uniformly on the surface of the gold substrate. Similarly, fluorescence intensities of Cy5-labeled ZZ-BNCs are in good agreement with the results obtained by QCM (Fig. 3, 3rd and 4th lines) (correlation coefficient, 0.988). Taken together, the binding of ZZ-BNCs might depend on the orientation of IgGs rather than the surface density of IgGs.

Discrimination of IgGs fixed in a randomized- and oriented-immobilization manner by ZZ-BNCs

In order to investigate the higher affinity of ZZ-BNCs for Ag–dIgG complexes, immunocomplexes of Ag and dIgG (Ag : dIgG = 4.9 : 7.5 in weight) were prepared in advance, adsorbed onto gold substrates, blocked with 0.2% Block Ace, and then brought into contact with ZZ-BNCs (Fig. 3, row D and ESI Fig. 1Q†). Compared with the sequential addition of Ag and dIgGs (Fig. 3, row A and ESI Fig. 1H†), the height and weight of gold substrates were moderately increased by the addition of ZZ-BNCs (to 8.42 ± 0.71 nm and by 252.0 ± 50.4 ng cm^{-2}, respectively). The weight ratio (2.56) of bound ZZ-BNCs to the dIgG moiety (60.5% of total weight) of bound Ag–dIgG immunocomplexes (Fig. 3, row D) was about one-third of the weight ratio (10.8) of bound ZZ-BNCs to cIgGs (Fig. 3, row A). As previously demonstrated,[22] dIgGs can be fixed onto a solid phase through their Fv regions in an "Ag-dependent oriented-immobilization manner". More precisely, the Fv regions of dIgGs were tethered onto solid-phase Ags such that the Fc regions of dIgGs were presented outwardly, away from the solid

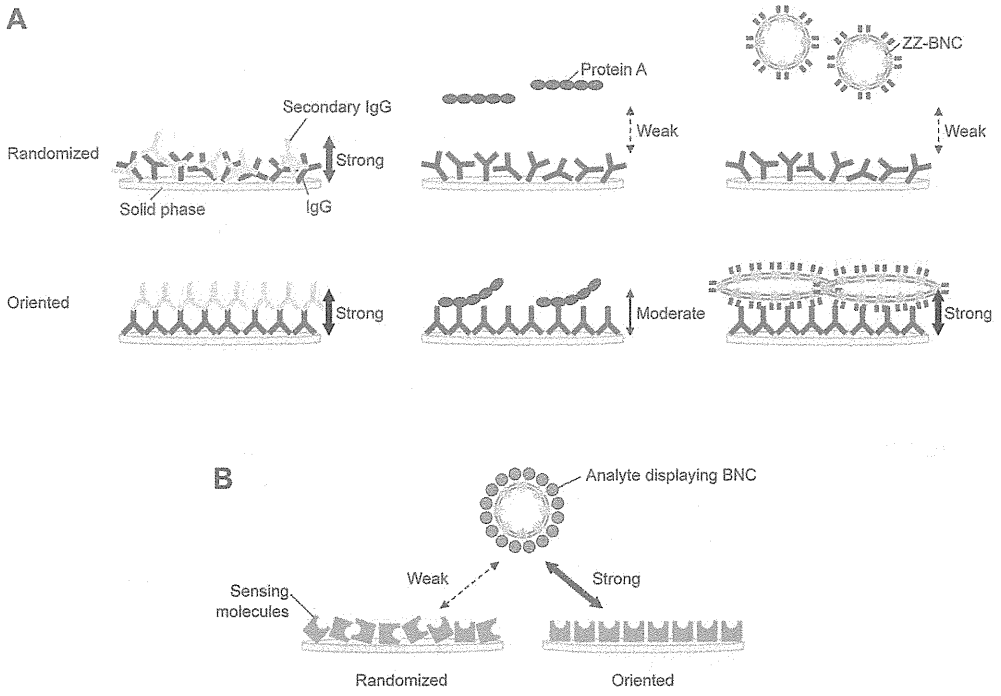

Fig. 4 Mode of function of ZZ-BNCs. (A) Postulated mechanisms for discriminating IgGs on a solid phase. IgGs fixed in a randomized- (upper panels) and oriented-immobilization manner (lower panels). Secondary antibodies (left panels), protein A (center panels), and ZZ-BNCs (right panels). (B) Concept for evaluating the direction of sensing molecules on a solid phase by BNCs displaying analytes.

phase. Our results therefore strongly suggested that ZZ-BNCs could detect the IgGs immobilized by Ags more efficiently than the randomly immobilized IgG–Ag complexes.

Orientation-specific detection of IgGs on a solid phase by ZZ-BNCs

The mechanisms underlying the specific recognition of IgGs fixed in an oriented-immobilization manner could be attributed to both the radial extension of Fc-binding Z domains on ZZ-BNCs and the large size of the ZZ-BNCs. First, since the display of Z domains was achieved in an oriented-immobilization manner and at a high density (approximately 72 800 molecules μm^{-2}), we considered that ZZ-BNCs would have a higher avidity for Fc regions fixed in an oriented-immobilization manner and at a comparable high density, rather than for those fixed in a randomized-immobilization manner and at low density. Furthermore, due to the surface of the solid phase, the shape of the BNCs spontaneously changed from spherical to dome shaped (oblateness: 4.33 ± 0.26) without disrupting its nanocapsule structure.[16] When the topographical images of ZZ-BNCs on the immunocomplexes were analyzed by AFM, ZZ-BNCs in Fig. 3 (rows A–D) were dome-shaped nanocapsules (oblateness: 7.61 ± 1.05, 6.15 ± 0.28, 7.03 ± 0.95 and 5.53 ± 0.56 [n = 6], respectively), suggesting that the absorption of ZZ-BNCs to the solid phase was additively enhanced by the immunocomplexes. Even when the surface of the solid phase was rugged, ZZ-BNCs could achieve optimal binding to Fc regions by changing their shape (Fig. 3, rows A, C and D, bottom line). Secondly, ZZ-BNCs are approximately 30 nm nanocapsules (of about 6500 kDa);[16] therefore, the steric hindrance around Z domains is assumed to be higher than that around Fv regions of secondary antibodies (approximately 10 nm, and about 150 kDa).[23] As shown in Fig. 4A, the Fc regions of IgGs that had been immobilized randomly (including cIgGs in Fig. 1B) are likely to be located in the vicinity of the solid phase and to be surrounded by flanking Fab regions. Hence, ZZ-BNCs could more efficiently recognize Fc regions of IgGs fixed in an oriented-immobilization manner (including cIgG–Ag–dIgG complexes in Fig. 1B) than Fc regions that had been randomly immobilized (Fig. 4A, right panels). In contrast, secondary antibodies were so small that they could interact with IgGs fixed in either an oriented- or a randomized-immobilization manner (Fig. 4A, left panels), abolishing the signals from cIgG–Ag–dIgG complexes with high background (see Fig. 1B). As for the complex of biotinylated protein A, biotinylated HRP, and avidin, the size of the complex (approximately 30 nm long for the 42 kDa protein A),[24] as well as of ZZ-BNCs, may allow it to interact specifically with the Fc regions of IgGs fixed in an oriented-immobilization manner (Fig. 4A, center panels). However, the number of Fc-binding domains (Z domains) in one complex is much smaller than that of ZZ-BNCs (about 5 compared to about 240), which may reduce the sensitivity of a sandwich ELISA using the complex (see Fig. 1B).

Conclusions

The radial extension of Fc-binding domains on ZZ-BNC facilitated the discrimination of IgGs fixed in an oriented- and randomized-immobilization manner, which allowed us to evaluate the direction of IgGs. The use of ZZ-BNCs as biosensing

molecules would not only allow the use of the same IgGs as cIgGs and dIgGs simultaneously in sandwich immunoassays, but would also improve the optimization of immunosensors significantly. Moreover, it would be promising to apply the ZZ-BNC-based technology for evaluating the direction of various sensing molecules (*e.g.*, receptors, ligands, lectins, sugars) on a solid phase by analyte-displaying BNCs (Fig. 4B). The BNCs displaying exogenous molecules (*i.e.*, analytes) could be generated by recombinant DNA techniques[13,25] and chemical modification.[26] Thus, it is anticipated that BNCs will be a unique probe for the evaluation of the orientation of sensing molecules on solid phases.

Acknowledgements

This work was supported in part by KAKENHI Grant-in-Aid for Scientific Research (A) (21240052 and 25242043, to SK); Grant-in-Aid for Young Scientists (B) (23710143 and 25870310, to MI), the Program for Promotion of Basic and Applied Researches for Innovations in Bio-oriented Industry (BRAIN; to SK), and the Health Labor Sciences Research Grant from the Ministry of Health Labor and Welfare (to SK).

References

1 T. A. Bendikov, A. Rabinkov, T. Karakouz, A. Vaskevich and I. Rubinstein, *Anal. Chem.*, 2008, **80**, 7487.
2 Z. Lv, J. Wang, G. Chen and L. Deng, *Int. J. Biol. Macromol.*, 2010, **47**, 661.
3 F. Liu, M. Dubey, H. Takahashi, D. G. Castner and D. W. Grainger, *Anal. Chem.*, 2010, **82**, 2947.
4 H. Y. Song, X. Zhou, J. Hobley and X. Su, *Langmuir*, 2011, **28**, 997.
5 X. Zhao, F. Pan, B. Cowsill, J. R. Lu, L. Garcia-Gancedo, A. J. Flewitt, G. M. Ashley and J. Luo, *Langmuir*, 2011, **27**, 7654.
6 Y. M. Bae, B. K. Oh, W. Lee, W. H. Lee and J. W. Choi, *Biosens. Bioelectron.*, 2005, **21**, 103.
7 M. Iijima, M. Somiya, N. Yoshimoto, T. Niimi and S. Kuroda, *Sci. Rep.*, 2012, **2**, 790, DOI: 10.1038/srep00790.
8 A. Kausaite-Minkstimiene, A. Ramanaviciene, J. Kirlyte and A. Ramanavicius, *Anal. Chem.*, 2010, **82**, 6401.
9 Z. Balevicius, A. Ramanaviciene, I. Baleviciute, A. Makaraviciute, L. Mikoliunaite and A. Ramanavicius, *Sens. Actuators, B*, 2011, **160**, 555.
10 J. R. Crowther, in *Molecular Biomethods Handbook*, ed. R. Rapley and J. M. Walker, Humana Press Inc, Totowa, 1998, p. 595.
11 S. Kuroda, S. Otaka, T. Miyazaki, M. Nakao and Y. Fujisawa, *J. Biol. Chem.*, 1992, **267**, 1953.
12 B. Nilsson, T. Moks, B. Jansson, L. Abrahmsén, A. Elmblad, E. Holmgren, C. Henrichson, T. A. Jones and M. Uhlén, *Protein Eng.*, 1987, **1**, 107.
13 N. Kurata, T. Shishido, M. Muraoka, T. Tanaka, C. Ogino, H. Fukuda and A. Kondo, *J. Biochem.*, 2008, **144**, 701.
14 M. Iijima, T. Matsuzaki, H. Kadoya, S. Hatahira, S. Hiramatsu, G. Jung, K. Tanizawa and S. Kuroda, *Anal. Biochem.*, 2010, **396**, 257.
15 M. Iijima, T. Matsuzaki, N. Yoshimoto, T. Niimi, K. Tanizawa and S. Kuroda, *Biomaterials*, 2011, **32**, 9011.
16 M. Iijima, H. Kadoya, S. Hatahira, S. Hiramatsu, G. Jung, A. Martin, J. Quinn, J. Jung, S. Y. Jeong, E. K. Choi, T. Arakawa, F. Hinako, M. Kusunoki, N. Yoshimoto, T. Niimi, K. Tanizawa and S. Kuroda, *Biomaterials*, 2011, **32**, 1455.
17 N. E. Coe Clough and P. J. Hauer, *ILAR J.*, 2005, **46**, 300.
18 J. Jung, M. Iijima, N. Yoshimoto, M. Sasaki, T. Niimi, K. Tatematsu, S. Y. Jeong, E. K. Choi, K. Tanizawa and S. Kuroda, *Protein Expression Purif.*, 2011, **78**, 149.
19 G. Z. Sauerbrey, *Z. Phys.*, 1959, **155**, 206.
20 E. Lazarides and B. D. Hubbard, *Proc. Natl. Acad. Sci. U. S. A.*, 1976, **73**, 4344.
21 D. MacDougall and W. B. Crummett, *Anal. Chem.*, 1980, **52**, 2242.
22 H. Yan, Z. Shen, R. Mernaough and X. Zeng, *Anal. Chem.*, 2011, **83**, 625.
23 N. H. Thomson, *Ultramicroscopy*, 2005, **105**, 103.
24 S. Ohnishi, M. Murata and M. Hato, *Biophys. J.*, 1998, **74**, 455.
25 T. Yamada, Y. Iwasaki, H. Tada, H. Iwabuki, M. K. L. Chuah, T. VandenDriessche, H. Fukuda, A. Kondo, M. Ueda, M. Seno, K. Tanizawa and S. Kuroda, *Nat. Biotechnol.*, 2003, **21**, 885.
26 T. Kasuya, J. Jung, H. Kadoya, T. Matsuzaki, K. Tatematsu, T. Okajima, E. Miyoshi, K. Tanizawa and S. Kuroda, *Hum. Gene Ther.*, 2008, **19**, 887.

Biosci. Biotechnol. Biochem., **77** (4), 120760-1–4, 2013

Note

Bio-Nanocapsules for Signal Enhancement of Alkaline Phosphatase-Linked Immunosorbent Assays

Masumi IIJIMA, Mikako YAMAMOTO, Nobuo YOSHIMOTO, Tomoaki NIIMI, and Shun'ichi KURODA†

Graduate School of Bioagricultural Sciences, Nagoya University, Nagoya, Aichi 464-8601, Japan

Received October 2, 2012; Accepted January 1, 2013; Online Publication, April 7, 2013
[doi:10.1271/bbb.120760]

The bio-nanocapsules displaying about 240 molecules of immunoglobulin G Fc-binding Z domains (ZZ-BNCs) enhanced the signals of enzyme-linked immunosorbent assay by tethering the Fc regions of secondary antibodies (Abs), which were eliminated using high-molecular mass enzymes (*e.g.*, alkaline phosphatase). By way of optimizing the distance between enzymes and Abs, ZZ-BNCs improved sensitivity independently of enzymes.

Key words: bio-nanocapsules; alkaline phosphatase; horseradish peroxidase; oriented immobilization; cluster formation

Enzyme-linked immunosorbent assay (ELISA) is used to detect immunocomplexes in biological, clinical, and food samples. Two different strategies are applied to secondary antibodies (enzyme-conjugated Abs) in the aqueous phase to improve their sensitivity and specificity for detection. One strategy is to cluster of Abs or enzymes onto macromolecules to amplify the signal.[1,2] Another is to immobilize onto macromolecular scaffolds to improve the avidity and antigen recognition capability of the Ab by reducing steric hindrance around the Fv regions.[3,4] However, due to the challenges inherent in chemically modifying Abs in a residue-specific manner, neither of these strategies has yet accomplished fully oriented immobilization of Abs.[5]

To achieve clustering and fully oriented immobilization of secondary Abs on macromolecular scaffolds, we generated bio-nanocapsules (BNCs) consisting of a liposome and approximately 120 molecules of ZZ-L proteins (hepatitis B virus surface antigen L protein harboring immunoglobulin IgG Fc-binding Z domains derived from *Staphylococcus aureus* protein A). ZZ-BNC displays approximately 120 surface ZZ domains (equal to approximately 240 Z domains) (Fig. 1A)[6] with a capacity to capture about 60 mouse full-length IgG molecules, and to display all IgG Fv regions outwardly for effective antigen binding.[7] When ELISA was performed to detect ovalbumin (OVA) on solid phase using anti-OVA Abs and horseradish peroxidase (HRP)-conjugated secondary Abs, the addition of ZZ-BNCs to the aqueous phase significantly enhanced HRP-derived signals through the formation of so-called "BNC-based enzyme-Ab conjugates" (Fig. 1B, left panel).[8] We attributed this enhancement to both cluster formation and fully oriented immobilization of HRP-conjugated secondary Abs on ZZ-BNC scaffolds. On the other hand, since alkaline phosphatase (ALP) has good stability, high turnover numbers, a variety of substrates, and can be measured by changes in absorbance, fluorescence, or luminescence,[9] we made attempts to use ALP-conjugated secondary Abs under the same conditions. As shown in Fig. 1B (right panel), ZZ-BNCs were found unexpectedly to attenuate the ALP-derived signals. In this study, to expand on the possibility of ZZ-BNCs in ALP-based ELISA and HRP-based ELISA, we optimized the structure of BNC-based enzyme-Ab conjugates for use with ALP-conjugated secondary Abs.

The interactions between ZZ-BNCs and HRP and ALP-conjugated secondary Abs were examined by a quartz crystal microbalance (QCM). The sensor chip in the measuring bath was first treated with ZZ-BNCs (10 μg/mL as protein), blocked with skimmed milk (2 mg/mL), and incubated with HRP- or ALP-conjugated secondary Abs (10 μg/mL; $n = 3$). ZZ-BNCs bound to the sensor chip in quantities were estimated based on the initial frequency change ($\Delta F = -2{,}799 \pm 27$ Hz, equivalent to $1{,}679 \pm 16$ ng/cm^2). After blocking with skimmed milk, 842 ± 48 ng/cm^2 of HRP-conjugated secondary Abs was adsorbed onto the sensor chip (Fig. 1C, left panel). By contrast, ALP-conjugated secondary Abs did not affect the initial frequency change (2 ± 3 ng/cm^2; Fig. 1C, right panel). These results confirm that ZZ-BNCs did not interact with ALP-conjugated secondary Abs.

The aforementioned secondary Abs were prepared by chemical conjugation with glutaraldehyde (a bifunctional reagent, spacer arm length, 5 Å), which at times resulted in an increase in molecular heterogeneity and the steric bulk of the secondary Abs.[10] It has also been reported that steric hindrance by high-molecular mass enzymes affected the sensitivity, specificity, and stability of ELISA.[11] Due to the higher molecular mass of ALP (about 112 kDa *versus* about 40 kDa for HRP), the steric hindrance caused by the ALP functionality in secondary Abs might prevent interaction between the Fc regions and ZZ-BNCs. In conventional ELISA (without the use of ZZ-BNCs), longer distances between enzymes and Abs generate higher signals from secondary Abs.[12] Hence, we reacted ALP with bifunctional cross-linkers of varying length, as follows (Table 1): *N*-[ε-maleimidocaproyl-oxy]sulfosuccinimide ester (EMCS; spacer arm length, about 12 Å), maleimide-polyethylene glycol

† To whom correspondence should be addressed. Tel/Fax: +81-52-789-5227; E-mail: skuroda@agr.nagoya-u.ac.jp

Abbreviations: Abs, antibodies; ALP, alkaline phosphatase; BNC, bio-nanocapsule; ELISA, enzyme-linked immunosorbent assay; HRP, horseradish peroxidase; IgG, immunoglobulin G; OVA, ovalbumin; QCM, quartz crystal microbalance

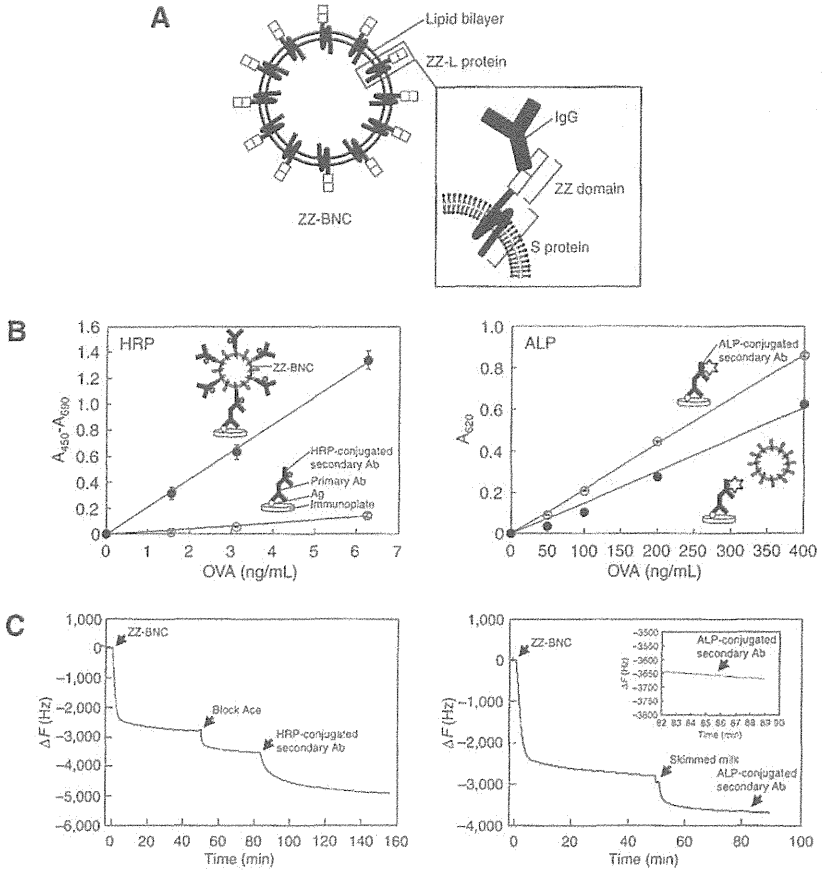

Fig. 1. Effects of Enzymes on the Interaction of Secondary Antibodies with ZZ-BNCs.

A, Capsular structure of ZZ-BNC. One ZZ-BNC particle consists of about 120 ZZ-L proteins embedded in a liposome. The ZZ domain and the S protein were necessary for interaction with the IgG Fc region and particle formation respectively. B, Detection of OVA (Sigma-Aldrich, St. Louis, MO) on solid phase by HRP- and ALP-based ELISA. OVA (100 μL at the indicated concentrations) was adsorbed to each well of a Nunc-Immuno Plate II (96 wells; Nalge Nunc International, Rochester, NY). The plate was kept at 4 °C overnight and washed 3 times with 200 μL of phosphate-buffered saline (PBS) containing 0.05% (v/v) Tween-20 (PBST). Abs were diluted with PBST containing 5% (w/v) skimmed milk (Nacalai Tesque, Kyoto, Japan). A primary Ab, a mouse anti-OVA IgG_1 (100 μL, 0.4 μg/mL; Abcam, Cambridge, UK), was added to each well, incubated at room temperature for 1.5 h, and washed 3 times with PBST. A secondary Ab, HRP- or ALP-glutaraldehyde-IgG (HRP- or ALP-conjugated rabbit anti-mouse IgG; 100 μL, 2 μg/mL; Sigma-Aldrich), was added to each well, incubated at room temperature for 1.5 h, and washed 3 times with PBST. In the case of the addition of ZZ-BNCs, the secondary Abs (2 μg/mL) were preincubated with ZZ-BNCs (2 μg/mL as protein) at room temperature for 30 min. The colorimetric reaction was performed at room temperature for 15 min in 100 μL per well of a 3,3′,5,5′-tetramethylbenzidine substrate kit (Pierce, Rockford, IL, for HRP) or a BluePhos microwell phosphatase substrate kit (Kirkegaard and Perry Laboratories, Gaithersburg, MD, for ALP). The reaction was stopped with 100 μL of 2 N H_2SO_4 (for HRP) or stop solution (for ALP). The absorbance at 450 nm (A_{450}) was measured on a Varioskan microplate reader (Thermo Fisher Scientific, Waltham, MA) using the absorbance at 690 nm and 620 nm as references for HRP and ALP respectively. Measurements were performed at least 4 times independently. Error bars indicate standard deviations. Solid circles, with ZZ-BNCs; hollow circles, without ZZ-BNCs. C, Interaction of ZZ-BNCs with HRP- and ALP-conjugated secondary Abs. The sensor chip of QCM (Twin-Q, As One, Osaka, Japan) consisted of a 9-mm diameter disk made from an AT-cut 27-MHz quartz crystal with gold electrodes on both sides (diameter, 2.5 mm; area, 4.9 mm^2). A frequency change (ΔF) of 1 Hz corresponded to a weight change of 0.6 ng/cm^2. The temperature of the measuring bath (500 μL) was kept constant at 25 °C with mixing at 600 rpm with a stirring tube. Measurements were performed until a stable frequency (less than ± 3 Hz) was observed for > 1 min in triplicate. The sensor chip was first treated with ZZ-BNCs (10 μg/mL as protein), and then blocked with skimmed milk (2 mg/mL). Finally it was reacted with HRP- or ALP-conjugated secondary Abs (10 μg/mL). Arrows separate steps between events.

(PEG)-carbonate-*N*-hydroxysuccinimide (NHS) (020TS, 050TS, and 400TS; spacer arm lengths, about 160 Å, about 400 Å, and about 3,100 Å respectively). The amine residues on the IgG surfaces (rabbit anti-mouse IgG) were converted to sulfhydryl residues by the catalytic action of *N*-succinimidyl *S*-acetylthioacetate (SATA), and then reacted with equimolar quantities of maleimide-containing ALPs. The molar ratio of ALP to IgG was estimated to be 1:1 for each ALP-conjugated IgG complex.

The binding capacities of ZZ-BNC to various ALP-conjugated IgGs (ALP-EMCS-IgG, ALP-020TS-IgG, ALP-050TS-IgG, and ALP-400TS-IgG) were measured by QCM (Table 1). HRP-glutaraldehyde-IgG but not ALP-glutaraldehyde-IgG exhibited a strong affinity for ZZ-BNCs (15.6 and 0 mol of IgG per mol of ZZ-BNC particles respectively), and the other ALP-conjugated IgGs displayed weak but comparable affinity for ZZ-BNCs (2.4–3.6 mol). These data strongly suggest that the increment of spacer arm length improved interaction between the IgG-Fc regions and the ZZ domains on the ZZ-BNCs, facilitating the formation of ALP-IgG-ZZ-BNC complexes. Next, ALP-conjugated IgGs prepared with longer cross-linkers were examined for their ability

Table 1. Effects of Spacer Arm Length of Secondary Abs on Binding Capacities of ZZ-BNCs

Antibodies[a]	Cross-linkers[a]	Enzymes[a]	Spacer arm length (Å)	Binding capacities (mol of IgG/mol of ZZ-BNC)[b]
IgG	Glutaraldehyde	HRP	5	15.6
IgG	Glutaraldehyde	ALP	5	0
SATA-IgG	EMCS	ALP	~12	3.6
SATA-IgG	020TS	ALP	~160	2.4
SATA-IgG	050TS	ALP	~400	2.4
SATA-IgG	400TS	ALP	~3,100	3.6

[a]Rabbit anti-mouse IgG (1 mg, Sigma-Aldrich) was reacted with a 10-fold molar excess of SATA (Pierce, Rockford, IL) at room temperature for 1 h. SATA-modified IgG (SATA-IgG) was deacetylated by 25 mM hydroxylamine at room temperature for 2 h to generate sulfhydryl-containing IgG. On the other hand, ALP (1 mg, Roche, Mannheim, Germany) was reacted with a 10-fold molar excess of cross-linkers (EMCS, Pierce; 020TS, 050TS, and 400TS, NOF, Tokyo) at room temperature for 30 min to generate maleimide-containing ALP. Sulfhydryl-containing IgG was reacted with an equal molar of maleimide-containing ALP at 4 °C overnight. The reaction was terminated with 2 mM 2-aminoethanethiol hydrochloride to obtain ALP-conjugated IgGs (ALP-EMCS-IgG, ALP-020TS-IgG, ALP-050TS-IgG, and ALP-400TS-IgG).

[b]The binding capacity of ZZ-BNC to the ALP-conjugated IgGs was determined by QCM ($n = 3$). The CV (coefficient of variation) for each value is less than 5%.

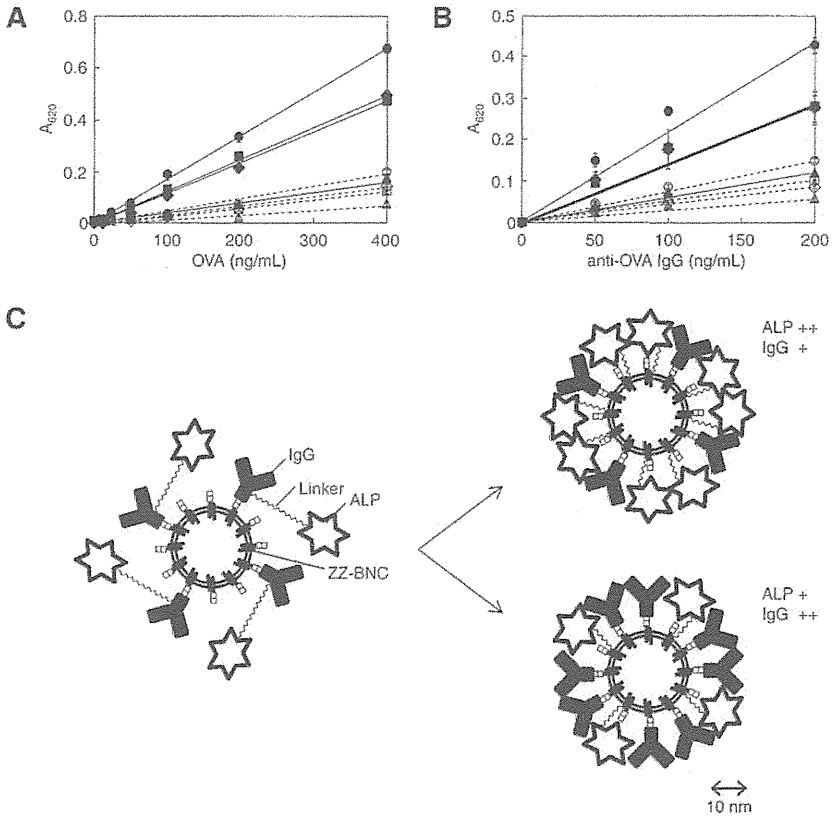

Fig. 2. Enhancement of ALP-IgG-Derived Signals by ZZ-BNCs.

A, Detection of OVA on solid phase by ELISA using various ALP-conjugated IgGs in the presence of ZZ-BNCs. As described in Fig. 1B, the amounts of OVA on solid phase were determined with ALP-EMCS-IgG (circles), ALP-020TS-IgG (squares), ALP-050TS-IgG (diamonds), and ALP-400TS-IgG (triangles), with and without ZZ-BNCs. Measurements were performed at least 4 times independently. Error bars indicate standard deviations. Solid symbols and bold lines, with ZZ-BNCs; hollow symbols and broken lines, without ZZ-BNCs. B, Detection of anti-OVA IgG in aqueous phase by ELISA using various ALP-conjugated IgGs in the presence of ZZ-BNCs. The OVA (100 μL, 400 ng/mL) adsorbed onto each well was contacted by anti-OVA IgG (100 μL, 0–200 ng/mL), followed by ALP-EMCS-IgG (circles), ALP-020TS-IgG (squares), ALP-050TS-IgG (diamonds), and ALP-400TS-IgG (triangles), with and without ZZ-BNCs. Measurements were performed at least 4 times independently. Error bars indicate standard deviations. Solid symbols and bold lines, with ZZ-BNCs; hollow symbols and broken lines, without ZZ-BNCs. C, Molecular organization of the new BNC-based ALP-Ab conjugates. ALP-conjugated IgGs were tethered onto ZZ-BNC in an oriented immobilization pattern (this study, left panel), which displayed at best four molecules of ALP-conjugated IgG on each ZZ-BNC. IgGs and ALPs were independently tethered onto ZZ-BNC in an oriented immobilization pattern and *via* longer spacer arms (12–100 Å) respectively (new model, right panel), which displayed >4 molecules of ALP and IgG at the optimal ALP/IgG ratio to accomplish maximum sensitivity.

to enhance ALP-derived signals for the detection of OVA on solid phase in the presence of ZZ-BNCs (Fig. 2A). By comparison with the signals obtained without ZZ-BNCs, the signals at 400 ng/mL OVA were increased 3.4-fold (ALP-EMCS-IgG), 4.0-fold (ALP-020TS-IgG), 4.0-fold (ALP-050TS-IgG), and 2.0-fold (ALP-400TS-IgG) upon the addition of ZZ-BNCs in aqueous phase. With sensitivity was defined by the limit of detection (LOD, mean ± 3 SD) and the limit of quantitation (LOQ, mean ± 10 SD) at the lowest end of the quantifiable concentration range of OVA (n = 20), LOD and LOQ of ELISA using ALP-020TS-IgG were significantly decreased by the addition of ZZ-BNCs from 200 pg/mL (CV = 5.2% for both), to 25 pg/mL (CV = 8.7%) and 50 pg/mL (CV = 4.2%) respectively. Furthermore, we investigated to determine whether the ALP-IgG-ZZ-BNC complexes contributed to the detection of anti-OVA IgGs in the aqueous phase (Fig. 2B). The signals at 200 ng/mL anti-OVA IgGs were 2.9-fold (ALP-EMCS-IgG), 2.7-fold (ALP-020TS-IgG), 3.3-fold (ALP-050TS-IgG), and 2.1-fold (ALP-400TS-IgG) higher than those without ZZ-BNCs.

These results confirm that the use of a variety of cross-linkers with longer spacer arms (>12 Å) facilitates the formation of ALP-IgG-ZZ-BNC complexes, thereby enhancing the sensitivity of conventional ALP-based ELISAs, presumably by oriented immobilization of IgGs. Since the average diameters of IgG and ALP are approximately 100 Å, the spacer arm length of glutaraldehyde (5 Å) is too short to present Fc regions on the surface of ALP-conjugated IgGs. This orientation makes it difficult for the ZZ domains of ZZ-BNC to slide into the cavity between IgG and ALP. However, even when longer spacer arms (>12 Å) were used, they did not further improve the interaction of ALP-conjugated IgGs with ZZ-BNC (Table 1). Meanwhile, the use of longer spacer arms made the interaction of ALP-IgG-ZZ-BNC complexes with primary Abs weaker, decreasing the sensitivity of ELISA (Fig. 2A and B). This result suggests that longer spacer arms consisting of PEG clustered on the surface of ALP-IgG-ZZ-BNC complexes formed hydrated phase around the Fv region of the secondary Ab portion and then repelled the access of primary Ab.[13] When 020TS and 050TS were used, sensitivity did not significantly change. Compared with 400TS, there is no substantial difference between the hydrated phases generated by the two PEG molecules. In sum, a spacer arm longer than the average diameter of IgG (100 Å) is inappropriate for ALP-IgG-ZZ-BNC complexes. For further optimization of the complexes, IgGs and ALPs should be displayed on ZZ-BNC directly in an oriented immobilization manner and indirectly with a 12–100 Å spacer arm respectively (Fig. 2C). This conformation should make it possible to optimize the ratio of IgG to ALP on ZZ-BNC.

Acknowledgments

This work was supported in part by the Grant-in-Aid for Scientific Research (KAKENHI, 21240052 to S.K. and 23710143 to M.I.), the Program for Promotion of Basic and Applied Researches for Innovations in Bio-oriented Industry (BRAIN) (to S.K.), and the Health Labour Sciences Research Grant from the Ministry of Health, Labour and Welfare of Japan (to S.K.).

References

1) Mora JR, Zielinski TL, Nelson BP, and Getts RC, *BioTechniques*, **44**, 815–818 (2008).
2) Zhou Y, Tian XL, Li YS, Pan FG, Zhang YY, Zhang JH, Yang L, Wang XR, Ren HL, Lu SY, Li ZH, Chen QJ, Liu ZS, and Liu JQ, *Biosens. Bioelectron.*, **26**, 3700–3704 (2011).
3) Teramura Y, Arima Y, and Iwata H, *Anal. Biochem.*, **357**, 208–215 (2006).
4) Grieshaber D, Lange VD, Hirt T, Lu Z, and Vörös J, *Sensors*, **8**, 7894–7903 (2008).
5) Rao SV, Anderson KW, and Bachas LG, *Mikrochim. Acta*, **128**, 127–143 (1998).
6) Kurata N, Shishido T, Muraoka M, Tanaka T, Ogino C, Fukuda H, and Kondo A, *J. Biochem.*, **144**, 701–707 (2008).
7) Iijima M, Kadoya H, Hatahira S, Hiramatsu S, Jung G, Martin A, Quinn J, Jung J, Jeong SY, Choi EK, Arakawa T, Hinako F, Kusunoki M, Yoshimoto N, Niimi T, Tanizawa K, and Kuroda S, *Biomaterials*, **32**, 1455–1464 (2011).
8) Iijima M, Matsuzaki T, Kadoya H, Hatahira S, Hiramatsu S, Jung G, Tanizawa K, and Kuroda S, *Anal. Biochem.*, **396**, 257–261 (2010).
9) Wisdom GB, "The Protein Protocols Handbook, 2nd Edition," ed. Walker JM, Humana Press, Totowa, pp. 343–344 (2002).
10) Avrameas S, *Immunochemistry*, **6**, 43–52 (1969).
11) Porstmann B, Porstmann T, Nugel E, and Evers U, *J. Immunol. Methods*, **79**, 27–37 (1985).
12) Bieniarz C, Husain M, Barnes G, King CA, and Welch CJ, *Bioconjug. Chem.*, **7**, 88–95 (1996).
13) Woodle MC, Newman MS, and Cohen JA, *J. Drug Target.*, **2**, 397–403 (1994).

SCIENTIFIC REPORTS

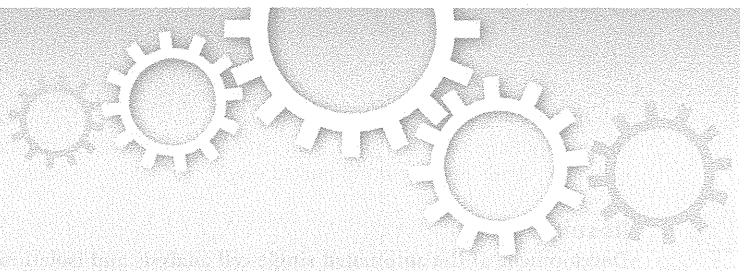

OPEN

SUBJECT AREAS:
ASSAY SYSTEMS
LAB-ON-A-CHIP
HIGH-THROUGHPUT SCREENING
BIOMATERIALS-CELLS

Received
25 October 2012

Accepted
17 January 2013

Published
1 February 2013

Correspondence and requests for materials should be addressed to N.Y. (n-yosi44@agr.nagoya-u.ac.jp) or S.K. (skuroda@agr.nagoya-u.ac.jp)

An automated system for high-throughput single cell-based breeding

Nobuo Yoshimoto[1,2], Akiko Kida[1], Xu Jie[3], Masaya Kurokawa[4], Masumi Iijima[1], Tomoaki Niimi[1], Andrés D. Maturana[1], Itoshi Nikaido[5], Hiroki R. Ueda[5], Kenji Tatematsu[2], Katsuyuki Tanizawa[2], Akihiko Kondo[6], Ikuo Fujii[7] & Shun'ichi Kuroda[1,2]

[1]Graduate School of Bioagricultural Sciences, Nagoya University, Furo-cho, Chikusa-ku, Nagoya, Aichi 464-8601, Japan, [2]The Institute of Scientific and Industrial Research, Osaka University, Mihogaoka, Ibaraki, Osaka 567-0047, Japan, [3]Furukawa Electric Co., Ltd., Yawata-kaigandori, Ichihara, Chiba 290-8555, Japan, [4]STARLITE Co., Ltd., Kamitoyama, Ritto, Shiga 520-3004, Japan, [5]Functional Genomics Unit, RIKEN Center for Developmental Biology, Minatojima-minamimachi, Chuo-ku, Kobe, Hyogo 650-0047, Japan, [6]Graduate School of Science and Technology, Kobe University, Rokkodai-cho, Nada-ku, Kobe, Hyogo 657-8501, Japan, [7]Graduate School of Science, Osaka Prefecture University, Gakuen-cho, Naka-ku, Sakai, Osaka 599-8570, Japan.

When establishing the most appropriate cells from the huge numbers of a cell library for practical use of cells in regenerative medicine and production of various biopharmaceuticals, cell heterogeneity often found in an isogenic cell population limits the refinement of clonal cell culture. Here, we demonstrated high-throughput screening of the most suitable cells in a cell library by an automated undisruptive single-cell analysis and isolation system, followed by expansion of isolated single cells. This system enabled establishment of the most suitable cells, such as embryonic stem cells with the highest expression of the pluripotency marker Rex1 and hybridomas with the highest antibody secretion, which could not be achieved by conventional high-throughput cell screening systems (*e.g.*, a fluorescence-activated cell sorter). This single cell-based breeding system may be a powerful tool to analyze stochastic fluctuations and delineate their molecular mechanisms.

Cell-based technology is sustained by a wide variety of cell species, such as bacteria, yeast, insect and plant, as well as animal and human cells, for research and industrial use. In particular, cells utilized in regenerative medicine and producing various biopharmaceuticals, such as cytokines, antibodies, enzymes, proteins, peptides and metabolites, have significantly contributed toward human welfare. For the practical use of biopharmaceuticals, it is essential to obtain the most appropriate cells from a candidate cell population. Thus far, conventional cell screening systems have been based on colony isolation by assuming all cells in a colony possess homogeneous characteristics[1,2]. However, recent single cell-based analyses have revealed that each cell in an isogenic cell population shows diverse and heterogeneous gene expression, morphology and/or cell proliferation[3–5]. For example, each cell of a mouse embryonic stem (ES) cell colony shows heterogeneous expression of the ES marker protein Rex1[6]. Humanized immunoglobulin G (IgG)-producing Chinese hamster ovary (CHO) cells are a mixture of clones showing stochastic fluctuations in IgG production[7]. Thus, a more rational approach has been considered necessary to isolate and culture the most suitable cells from a huge number of cell candidates by single-cell isolation and expansion (*i.e.*, single cell-based breeding). Although we have examined the use of a fluorescence-activated cell sorter (FACS) as a practical approach, the recovered cells suffered from mechanical stresses probably associated with high voltage and pressure, as well as chemical stress from the sheath solution for cell suspension. A conventional FACS system requires cell sample consisting of $\sim 1 \times 10^5$ cell population and containing more than 0.1% positive cells[8]. Considering the cell sample may be limited, a large portion of the sample is required for FACS optimization, in which cell sample is not recovered. These current issues of FACS technology prompted us to develop a novel system capable of isolating single positive cells from less than 1×10^5 cells under undisruptive conditions. In this study, we have developed an automated single-cell analysis and isolation system to facilitate high-throughput isolation of fluorescently labeled mammalian cells in an undisruptive and single cell-based manner. The robot is a stand-alone machine with a microchamber array chip (containing $\sim 2.5 \times 10^5$ cells) and an automated micromanipulator with a glass capillary and fluorescence microscope system, which isolates single positive cells from $\sim 2.5 \times 10^5$ cells under undisruptive conditions. Here, we report single cell-based selection and expansion of mouse ES cells with a homogeneous genetic background for

the pluripotency marker gene Rex1 and hybridomas that highly secrete antibody, using our automated single-cell isolation system.

Results

Development of the automated single-cell analysis and isolation system. Recently, a microchamber array chip was developed, which allows single-cell microarray analysis of a large cell population (~2.0 × 10^5 cells)[8]. Each microchamber (10 μm in diameter) is designed to accommodate only one cell and enables weak fluorescence detection at a high signal to noise ratio by excluding noise signals from negative cells. However, both the fluorescence analysis and single-cell isolation of on-chip cells have been carried out manually. A fully automated single-cell isolation system may improve screening efficiency for the most appropriate cell from a candidate cell population. Therefore, we constructed a robot that executed the following procedures automatically. First, acquisition of the fluorescent intensity of each cell on the microchamber array chip. Second, permutation of cells by the order of their fluorescent intensities. Third, physical retrieval of desired cells with a glass capillary attached to a micromanipulator. Fourth, movement and release of isolated cells to the

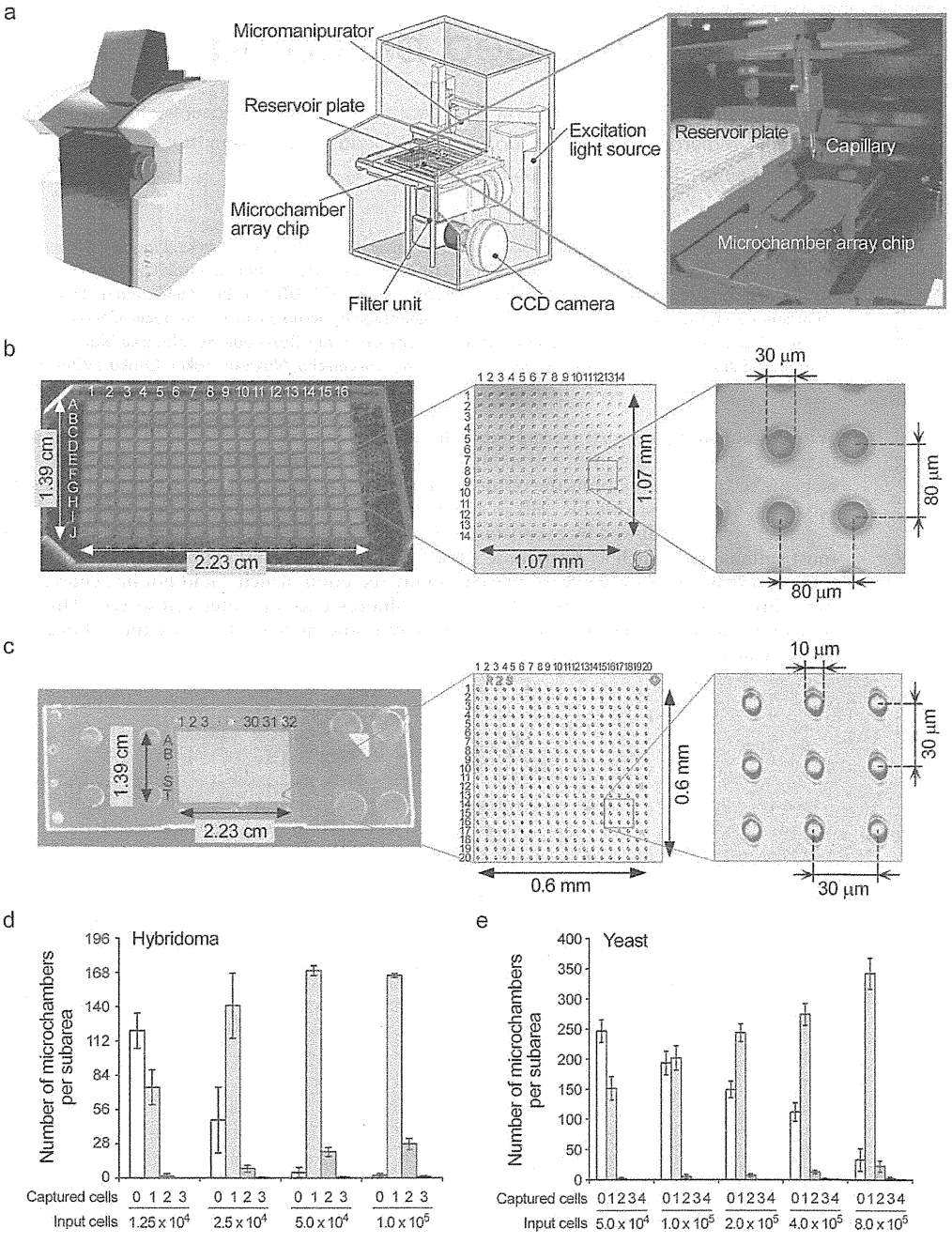

Figure 1 | Overview of the automated single-cell analysis and isolation system. (a) Automated single-cell analysis and isolation system. (b) Microchamber array chip made of polydimethylsiloxane (PDMS, 31,360 wells, 30 μm diameters). Left, overview (10 × 16 subareas); center, subarea (14 × 14 wells); right, wells. (c) Microchamber array chip made of polystyrene (PS, 256,000 wells, 10 μm diameters). Left, overview (20 × 32 subareas); center, subarea (20 × 20 wells); right, wells. (d) Cell numbers of hybridoma in each 30-μm PDMS microchamber. *Error bars* = SD (n = 6). (e) Cell numbers of yeast in each 10-μm PS microchamber. Cell numbers of hybridoma in each 30-μm PDMS microchamber. *Error bars* = SD (n = 6).

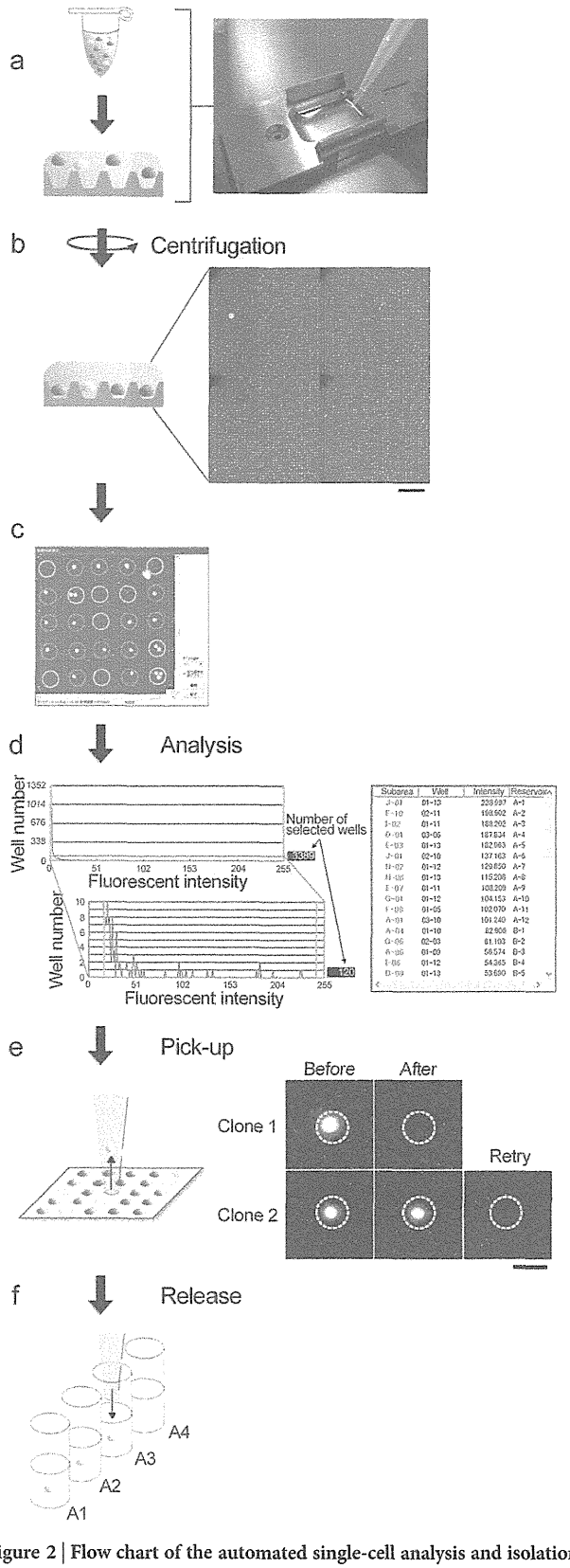

Figure 2 | Flow chart of the automated single-cell analysis and isolation system. Approximately 5.0×10^4 cells in culture medium were added to the microchamber array chip equipped with an aluminum frame (step (a)) and then introduced into 30-μm PDMS microchambers by brief centrifugation ($50 \times g$, at room temperature for 1 min) (step (b)). The microchamber array was scanned with a CCD camera on the robot. Based on the fluorescent image, microchambers containing no or more than 2 fluorescent particles were excluded from further analyses. Green circles, excluded microchambers; red circles, selected microchambers (step (c)). A histogram of fluorescent intensity from each cell was generated for permutation of cells by the order of fluorescent intensities, a list of addresses, fluorescent intensities and images, as well as a transmission image of each cell was generated (step (d)). Cells of interest were automatically retrieved with a glass capillary attached to the micromanipulator. Recovery of each cell was repeated until the fluorescence from each microchamber was absent (step (e)). Each retrieved cell was transferred to an assigned reservoir well (step (f)). *Scale bars* = 200 μm (b) and 30 μm (e).

reservoirs of a multi-well plate (Figure 1a). Detailed specifications of the robot were described in "Methods section." Two types of microchamber array chips were fabricated with polydimethylsiloxane (PDMS) for mammalian cells (31,360 wells on a 1.39×2.23 cm^2 total area; 30 μm diameter, 80 μm well-to-well pitch and 30 μm well depth) (Figure 1b), and with polystyrene (PS) for small mammalian or yeast cells (256,000 wells on a 1.39×2.23 cm^2 total area; 10 μm diameter, 30 μm well-to-well pitch and 10 μm well depth) (Figure 1c). Various numbers of hybridomas were introduced into 30-μm microchambers by brief centrifugation. Approximately 80 ~ 90% of microchambers were occupied by single hybridomas (Figure 1d). Similarly, yeast cells were introduced into 10-μm microchambers at comparable efficiency (Figure 1e).

Flowchart of the automated single-cell analysis and isolation system. Cell manipulation by the robot was carried out as follows. Cells were introduced into microchambers by brief centrifugation (Figure 2, steps a and b) and covered with culture medium, which could be cultured for at least 24 h. The fluorescent intensities of 9,600 microchambers on a chip were measured by the robot for 30 s (14 min for a 256,000 microchamber array chip) (step b; Supplementary video S1 online). Microchambers containing no or more than 2 fluorescent particles were excluded from further analyses (step c). Finally, a histogram together with a list of correlations between the position and fluorescent intensity of each cell was generated (step d). Cells of interest could be virtually marked in a descending/ascending/random order of fluorescent intensity. Marked cells were automatically collected with a glass capillary attached to the micromanipulator of the robot, which were confirmed by elimination of fluorescence in the target microchamber (step e). Upon failure, the robot automatically repeated the collection process. Each cell was transferred and released into the culture medium of an assigned well in 96- or 384-well plates (step f). The reciprocal movement of the glass capillary required 15 s for each cell (Supplementary video S2 online).

Single cell-based breeding of mouse ES cells. Among established ES cell lines, the expression of pluripotency markers in each cell has often been observed in a stochastic fluctuating state[3,6]. When ~5.0×10^4 cells of the mouse ES cell line OLG harboring the Oct4-EGFP gene were introduced to 30-μm PDMS microchambers in our system, the cells showed variety of expression level of Oct4 (Figure 3a, upper panel). The mouse ES cell line clone No. 10 harboring the Rex1-EGFP gene showed an even higher degree of variety of expression level of Rex1 (Figure 3a, lower panel), indicating that each mouse ES cell line showed a distinct distribution of stemness[9]. From the cell library of clone No. 10 mouse ES cells, 24 cells with the highest fluorescent intensity were transferred to culture medium and allowed to proliferate from 1 to ~1,000 cells over 7 d (Figure 3b). The daughter cells formed rounder colonies with increased homogeneous Rex1-EGFP expression, compared with that of parental cells. After 2–3 weeks, 23 clones reached ~1×10^6 cells, in which

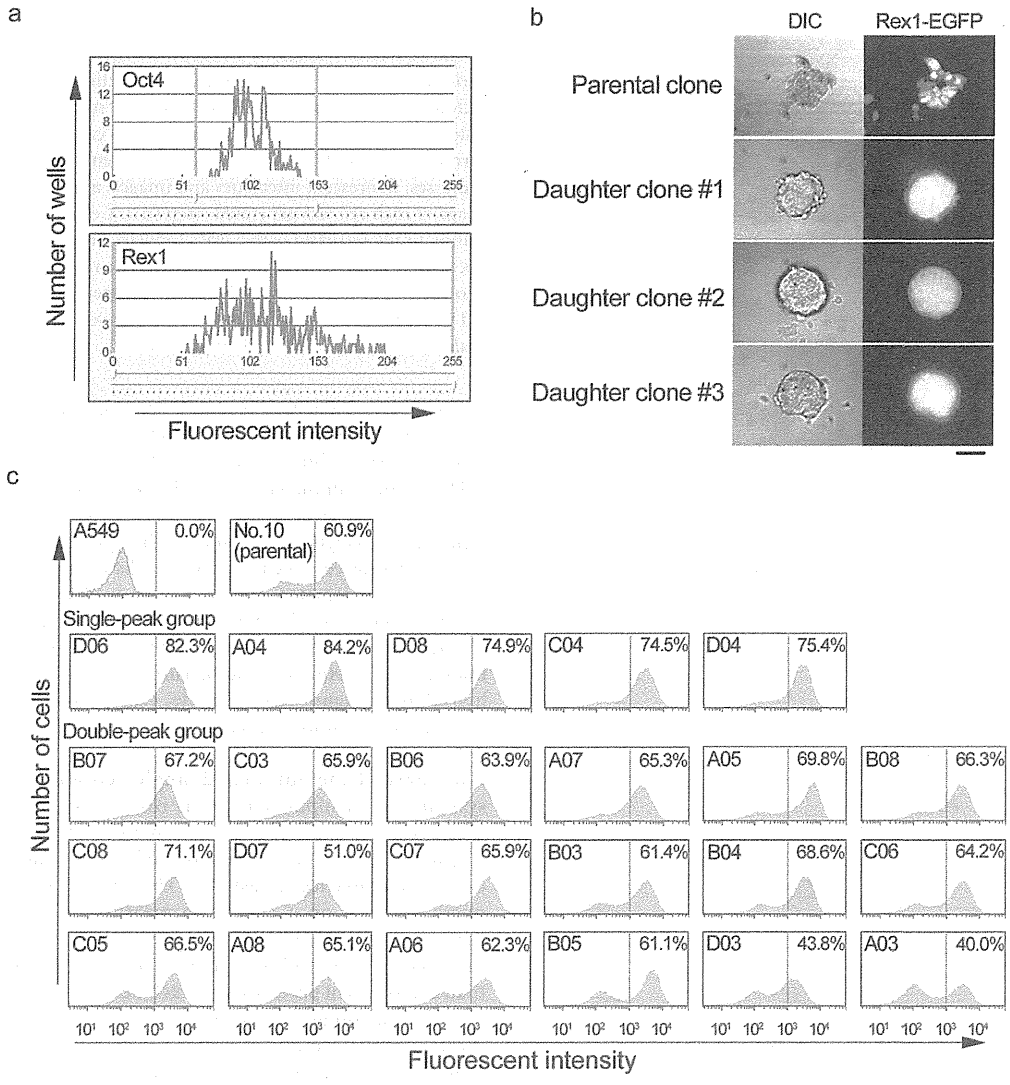

Figure 3 | Single cell-based breeding of mouse ES cells. (a) Oct4-EGFP and Rex1-EGFP expression in mouse ES cell lines OLG and No. 10, respectively, were analyzed by the robot. (b) Colony formation from isolated No. 10 cells (daughter cells). *Scale bar* = 50 μm. (c) Rex1-EGFP expression of isolated No. 10 cells. Approximately 2.0×10^4 cells were analyzed by FACS. Clone numbers are indicated in the upper-left. Contents of cells with higher fluorescent intensity (over 10^3) are indicated in the upper-right. A549 (an adenosquamous lung carcinoma cell line) cells were used as a negative control.

20 clones retained a higher fluorescent intensity compared with that of the parental cell population (Figure 3c). When calculating the ratio of highest numbers of cells with higher intensity (over 10^3) to those with lower intensity ($10^2 \sim 2 \times 10^2$), the daughter cells of >7.0 ratio (mean + 3SD of parental cells, n = 6) were judged as a single-peak group. Finally, we obtained 5 clones expressing higher level of Rex1, which would be suitable for further breeding process (Figure 3c). This result indicated that single cell-based breeding of cells isolated from a cell library is a powerful method to expand ES cells with the highest expression of pluripotency markers. ES and induced pluripotent stem (iPS) cells, particularly from humans, are often susceptible to mechanical and chemical stresses[10]. The automated single-cell isolation system is practical for isolating suitable cells under undisruptive conditions because of gentle manipulation of cells in culture medium with a glass capillary.

Single cell-based breeding of hybridomas. To evaluate the secretion of anti-rabbit lactate dehydrogenase IgG_1 from the hybridoma cell line HyLDH/YK-1, we treated the hybridomas with brefeldin A (a protein transport inhibitor)[11] to accumulate the IgG intracellularly, followed by FACS analysis. The isogenic cells were found to secrete various amounts of antibody and showed a dynamic fluorescent intensity range between $\sim 10^2$ and $\sim 10^5$ (Figure 4a). A traditional limiting dilution method to isolate mammalian cells secreting high amounts of biopharmaceuticals, deposits the cell library into 96- or 384-well plates at ~1 cell per well to form colonies. After culturing for at least 1 month, the supernatants of these cell cultures are assayed by enzyme-linked immunosorbent assay (ELISA) to detect candidate clones, followed by establishing the selected cells, which is time consuming with low scalability (up to ~100 candidate clones per screen). Recently, two automatic single-colony isolation systems became commercially available (ClonePix FL (Molecular Devices, Sunnyvale, CA, USA) and CellCelector (AVISO, Jena, Germany)). Both machines facilitate manipulation of a large number of cells, but approximately 1 month is still required for colony formation and identification of candidate cells[12,13]. Using a cuboid microchamber array as the single-cell container and the solid phase of the ELISA, candidate cells can be manually detected after culturing cells for

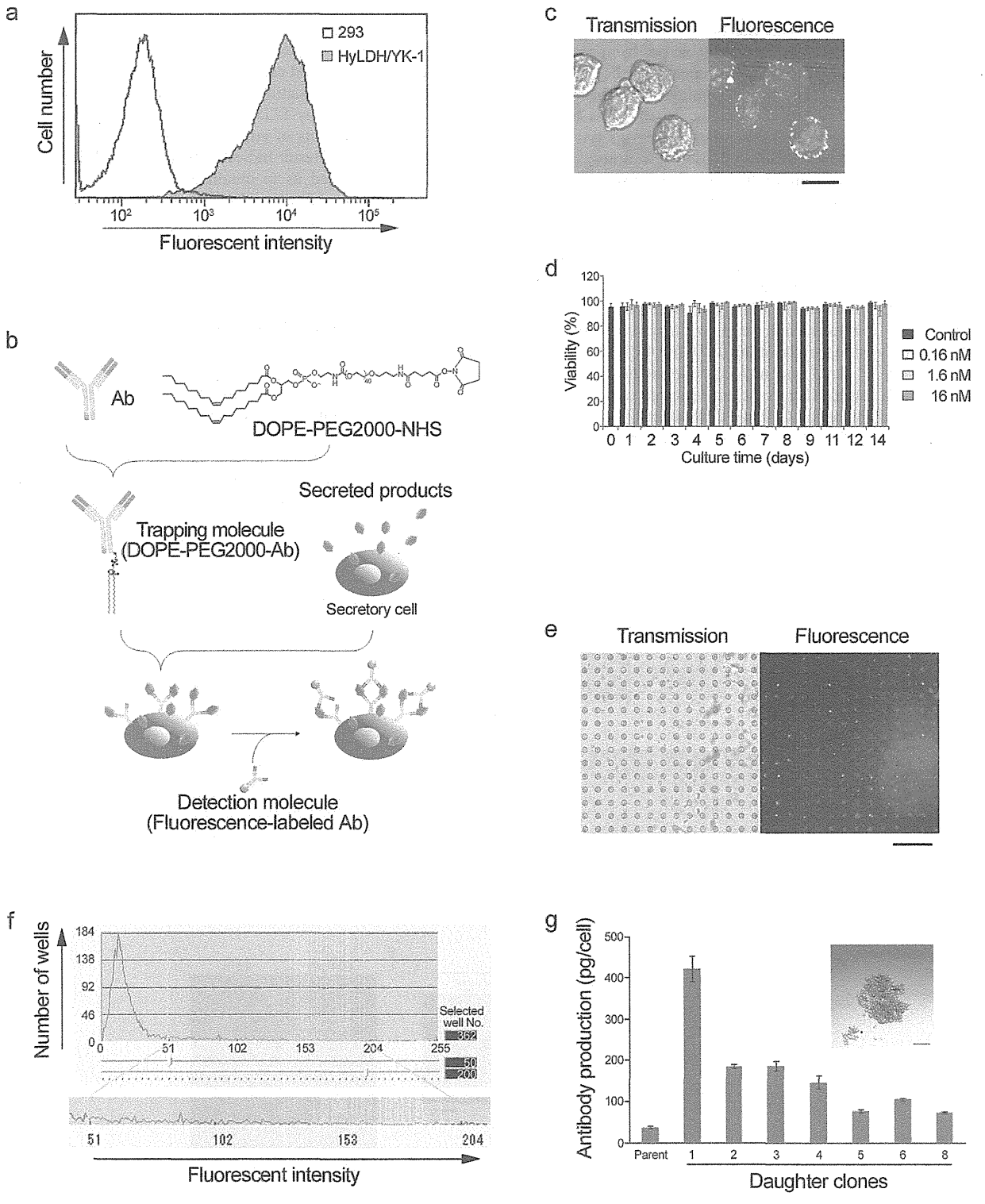

Figure 4 | Single cell-based breeding of hybridomas. (a) Antibody production by mouse hybridoma HyLDH/YK-1 cells was analyzed by FACS. HEK293 cells were used as a negative control. (b) Outline of the cell-surface FIA. Cells displaying trapping molecules, goat anti-mouse Fc antibody conjugated to DOPE-PEG2000, were allowed to capture secreted antibodies and then treated with a FITC-labeled rabbit anti-mouse $F(ab')_2$ antibody for detection. (c) Alexa 488-labeled trapping molecules on the surface of HyLDH/YK-1 cells. *Scale bar* = 20 μm. (d) Cytotoxicity of the trapping molecule on HyLDH/YK-1 cells. Cell viabilities were measured by trypan blue staining; *error bars*, $p < 0.01$, n = 12 from three independent experiments. (e) On-chip cell-surface FIA visualized by the robot. *Scale bar* = 240 μm. (f) Histogram of antibody secretion determined by the cell-surface FIA. Black vertical lines indicate fluorescence thresholds (range 50–200). White vertical lines indicate cells with high fluorescent intensities. (g) Antibody secretion determined by a conventional ELISA. Seven cells formed colonies at ~10 d after single-cell isolation (inset, *scale bar* = 100 μm) and were subjected to ELISA at ~20 d. *Error bars*, $p < 0.05$, n = 6 from three independent experiments.

several days. The selected cells are then automatically isolated by CellCelector[13]. However, both machines are unable to promptly and automatically isolate the most suitable cell from a cell library, and retain the issue of cell heterogeneity in the isogenic cell population. Meanwhile, an automated single cell isolation system (Cellporter system; SC World, Toyama, Japan)[14] has been developed, which is likely to utilize similar picking-up system to our study. But, the machine requires additional scanning system (SC Scanner) for measurement of fluorescent intensity of each cell, indicating that Cellporter system is not a completely automated system for cell analysis and isolation. To identify hybridomas that secreted higher amounts of antibodies, we developed an undisruptive cell-surface fluorescence-linked immunosorbent assay (CS-FIA) to evaluate antibody production at a single-cell level using the robot (Figure 4b). The surfaces of secreting cells were modified with a goat anti-mouse Fc antibody conjugated to dioleoyl phosphatidylethanolamine-poly-ethylene glycol 2000 (DOPE-PEG2000) as a trapping molecule[15,16]. Trapping molecules spontaneously assembled around the cell surface (Figure 4c) and showed no cytotoxicity for at least 2 weeks (Figure 4d). Cells were introduced into 30-μm PDMS microchambers to allow the capture of secreted antibodies at the cell surface, followed by incubation with a fluorescein isothiocyanate (FITC)-labeled rabbit anti-mouse $F(ab')_2$ $F(ab')_2$ to establish the sandwich FIA on the cell surface (Figure 4e). After analyzing on-chip cells using the robot, 362 cells exhibited higher fluorescence among the $\sim 5.0 \times 10^4$ cells (Figure 4f). Eight cells with the highest level of fluorescence were isolated. Seven cells formed colonies within 10 d and expanded to $\sim 5 \times 10^5$ cells over 2 weeks (Figure 4g). When evaluating the amount of antibody secreted into the culture medium by ELISA, the daughter cells were found to secrete higher amounts of antibodies, compared with that of the parental clone. This result indicated that single cell-based analysis and isolation allowed us to obtain hybridomas with the highest antibody-secreting ability in only 1 day. Because the CS-FIA technique is applicable to other cell types and various secreted biomaterials, the combination of the automated single-cell isolation system with the CS-FIA would be more effective to improve the productivity of biomaterials secreted from various cells.

Single cell isolation of adhesive cells. Since ES cells and hybridomas are less adhesive and non-adhesive cells, respectively, we herein examined if the robot is applicable to adhesive cells, such as CHO cells. CHO cells ($\sim 1.0 \times 10^4$ cells) were trypsinized, stained with CytoRed (fluorescent dye for viable cells; Dojin, Kumamoto, Japan) and then introduced into 30-μm PDMS microchambers at comparable efficiency of ES cells and hybridomas (Figure 5a). Within 3 h, single CHO cells could be retrieved according to their fluorescent intensities by the robot (Figure 5b), and proliferate to ~4

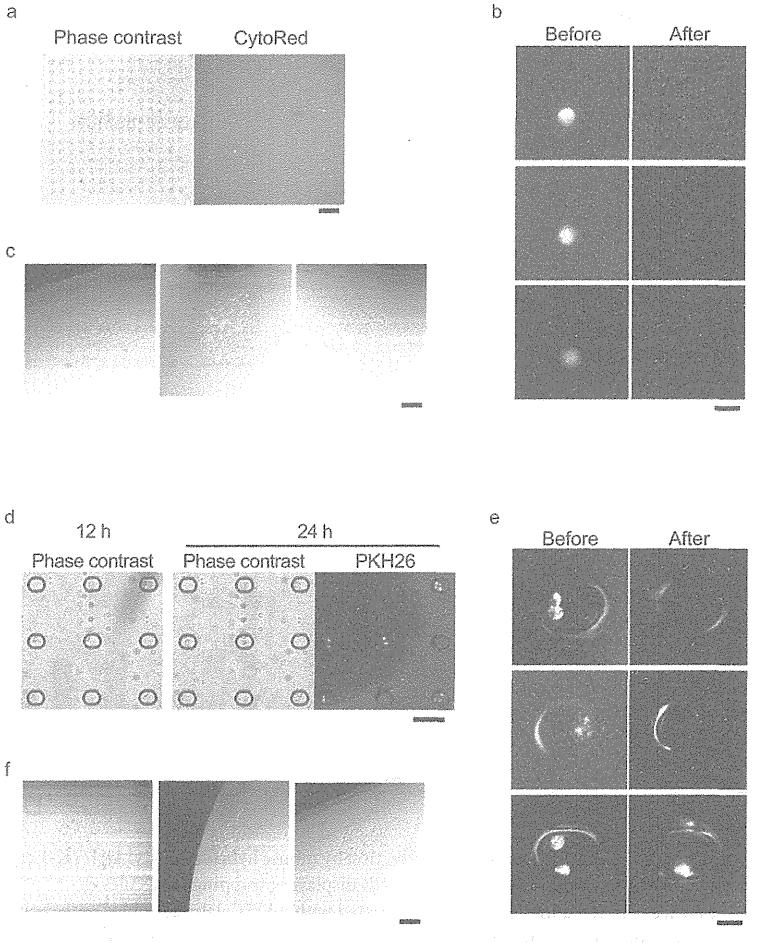

Figure 5 | Single cell isolation of CHO cells. (a) Cell array for CHO cells. Cells were stained with CytoRed solution. *Scale bar* = 160 μm. (b) Retrieval of single CHO cell. *Scale bar* = 25 μm. (c) Colony formation from isolated CHO cells. *Scale bar* = 200 μm. (d) On-chip culture of CHO cells. Cells were cultured on microchamber array chip and stained with PKH26. *Scale bar* = 100 μm. (e) Retrieval of cell cluster of CHO cells. CHO cells stained with PKH26 were trypsinized and retrieved with the robot. *Scale bar* = 25 μm. (f) Colony formation from isolated cell cluster of CHO cells. *Scale bar* = 200 μm.

$\times 10^2$ cells in 6 days (Figure 5c), of which the viability was more than 80% of retrieved single cells (20/24 clones). Furthermore, single CHO cells transferred into 50-μm ellipsoidal PS microchambers could propagate to several cells in microchambers (Figure 5d). After 24 h, the cells were stained with PKH26 (fluorescent dye for membrane staining; Sigma-Aldrich, St Louis, MO, USA), trypsinized briefly, and then retrieved as a cell cluster by the robot (Figure 5e). These cell clusters were allowed to grow up to $\sim 2 \times 10^2$ cells in 5 days (Figure 5f), of which the viability was nearly 100% of retrieved cell clusters (10/10 cell clusters). The automated retrieval of cell clusters might be useful for the single cell-based breeding of vulnerable adhesive cells.

Discussion

To manufacture biopharmaceuticals, each cell used for production (*e.g.*, hybridomas and CHO cells) should express biomaterials stably and efficiently. In regenerative therapies, each stem cell should express pluripotency markers homogeneously to obtain differentiated cells with less tumorigenicity. It is an important step to isolate the most suitable cell from a candidate cell library and expand the cell population for further optimization. However, both isolation and expansion have been traditionally performed with a cell colony, which impairs isolation of suitable cells because of potential difficulties in excluding contaminating unsuitable cells. Furthermore, long-term culture necessary for colony formation often impairs the favorable properties of isolated cells[7]. For example, the productivity of established hybridomas is sometimes decreased by long-term cell culture[17]. In established ES, iPS and mesenchymal stem cells, a trace number of cells in colonies cannot fully differentiate, which sometimes leads to severe tumorigenesis[18,19]. These cellular instabilities are mainly caused by stochastic fluctuation of gene expression among individual cells[3–7], which is considered a general phenomenon in various cell types. Although cellular instabilities have been conventionally circumvented by contingency-based cell screenings (*i.e.*, random screening of naturally occurring suitable cells) to establish cells with low stochastic fluctuation, the molecular mechanisms underlying stochastic fluctuation should be delineated. For example, after purifying two types of cells with high and low stochastic fluctuation by single-cell isolation, a comparison of gene expression profiles might delineate the mechanisms. Taken together, cells used for producing biopharmaceuticals and regenerative therapies should be established by single cell-based screening to maximize favorable properties and minimize the occurrence of stochastic fluctuation.

Here, we demonstrated that an automated single-cell isolation system facilitates prompt and effective establishment of the most suitable single cells from a large number of candidate cells to avoid the occurrence of stochastic fluctuation. Mouse ES cells with the highest expression level of the pluripotency marker Rex1 were successfully isolated from a heterogeneous cell population. Although 3 isolated ES cells (clones D07, A03, D03) showed lower expression level of Rex1 at 2–3 weeks after single-cell isolation, 20 cells retained higher Rex1 expression (*see* Figure 3c). Particularly, 5 isolated ES cells (clones D06, A04, D08, C04, D04) were found to show homogeneous profile of Rex1 expression. In addition, hybridomas secreting the highest amount of antibodies were isolated by the robot in combination with a CS-FIA technique. All isolated hybridomas showed a higher expression level of antibody than that of parental hybridomas at ~21 days after single-cell isolation (*see* Figure 4g). These results indicate that single cell-based breeding is a practical way to obtain suitable cells with fewer effects from stochastic fluctuation. Moreover, these established cells would be useful to decipher the molecular basis of stochastic fluctuation.

Micromanipulation under a microscope, limiting dilution and FACS have been widely used to isolate single cells. Micromanipulation is undisruptive and reliable for manipulating single cells, but extremely laborious. Limiting dilution is also undisruptive, but not reliable because of possibly excluding suitable cells during serial dilutions. As described in the introduction, FACS is a high-throughput and reliable system for isolating cell populations, but cannot isolate a single positive cell from less than 1×10^5 cells under undisruptive conditions. In particular, the chemical and mechanical stresses intrinsically associated with FACS are likely to alter the gene expression profiles of isolated single cells, thus single-cell manipulation should be carried out under undisruptive conditions. The issues of these techniques for isolating single cells have led us to develop an automated single-cell isolation system. The robot is designed to isolate a single positive cell from less than 1×10^5 cells in about 1 ml of culture medium. Therefore, the automated single-cell isolation system is considered suitable for high-throughput single cell-based analysis and isolation.

In high-throughput identification of hybridomas that secrete high amounts of antibodies, candidate hybridomas can be selected by FACS, followed by colony formation and evaluation with a conventional ELISA. Cell-surface markers (*e.g.*, CD19, CD20, CD38, CD138)[20–24] expressed in hybridomas are indirectly labeled with fluorescence, and then populations of positive cells are collected as candidate hybridomas by FACS. This method cannot evaluate the antibody-secreting ability of each hybridoma directly, and only concentrates candidate hybridomas. Another method is treatment of cells with brefeldin A to accumulate antibodies intracellularly. This method can evaluate the antibody-secreting ability, but also severely affects cell viability. Thus far, no reported method can evaluate the antibody-secreting ability of hybridomas directly in an undisruptive manner and without the requirement of long-term culture for colony formation. Here, we developed a CS-FIA that fulfills the above criteria. Combination of the CS-FIA with the robot successfully shortened the time to identify positive hybridomas from ~1 month (FACS) or ~2 months (limiting dilution) to 1 day. To further optimize the CS-FIA, the use of fluorescence-labeled antigens as detection molecules could improve the signal to noise ratio by reducing cross reactions among displayed antibodies.

In addition to single cell-based high-throughput analysis and isolation, our robot can be used for the following applications. Because the robot can evaluate protein-protein interactions on the cell surface, orphan ligand screenings using cells displaying receptor libraries, and orphan receptor screenings using cells expressing cell surface-anchored forms of ligand libraries are applicable, which may lead to drug discovery. Moreover, because of the undisruptive condition during cell manipulation, the robot would be suitable for isolation of rare cells in limited clinical samples (*e.g.*, circulating tumor cells[25] and cancer stem cells[26]) to develop an innovative diagnosis system. Thus, our automated single-cell isolation system may offer a new technology for single cell-based engineering and bring significant progress to cell-based research and industries.

Methods

The automated single-cell analysis and isolation system. The robot consisted of a micromanipulator (<1 μm movement accuracy) equipped with a pencil pump (DENSO, Aichi, Japan) and glass capillary (40.5 μm inside diameter, 58 μm outside diameter for mammalian cell; 14.5 μm inside diameter, 21 μm outside diameter for yeast cell), a CCD camera (Nikon, Tokyo, Japan), an objective lens (Plan Fluor 10 ×/0.3, Nikon), an excitation light source (Nikon) using a super high pressure mercury lamp and power supply, filter units (for FITC, 465–495-nm excitation, 515–555-nm emission, 505 nm dichroic mirror; for Cy3, 510–560-nm excitation, 572.5–647.5-nm emission, 565 nm dichroic mirror, Nikon), a 96- or 384-well reservoir plate, a microchamber array chip and a control PC (CPU, Pentium M 1.8 GHz; RAM 980 MB). Microfabrication on the polymethylmethacrylate (PMMA) plate was performed by X-ray mask and lithography technology combined with synchrotron radiation[8,27]. Using the patterned PMMA plate as a master plate, a nickel (Ni) mold part was produced by an electro-forming process resulting in effective production of the Ni mold part with replicated micro-patterns. Then, the mold part was inserted into a mold base and injected to produce a microchamber array chip with polystyrene or PDMS. The robot identified a minimum 1 μm single particle at <1800 MESF from the fluorescence of GFP, EGFP, phycoerythrin and propidium iodide. The control PC regulated the vertical movement of the micromanipulator, the horizontal movement

of the microchamber array chip, fluorescence acquisition and transmission of images to indentify cells of interest, followed by cell recovery using the pencil pump.

Cell culture. Mouse ES cell lines, OLG and clone No. 10, were cultured in Glasgow Minimum Essential Medium (Sigma-Aldrich, St Louis, MO, USA) supplemented with 10% fetal bovine serum (FBS; StemCell Technologies, Vancouver, BC, Canada), 1 mM sodium pyruvate, 0.1 mM non-essential amino acids (NEAA; Invitrogen Life Technology, Carlsbad, CA, USA), 32.7 mM sodium bicarbonate, 0.1 mM 2-mercaptoethanol and 1,000 U ml^{-1} leukemia inhibitory factor (Invitrogen). The mouse hybridoma cell line HyLDH/YK-1 secreting anti-rabbit lactate dehydrogenase IgG_1 was cultured in RPMI-1640 (Nacalai, Kyoto, Japan) supplemented with 10% FBS (Thermo, Waltham, MA, USA), 0.1 mM NEAA and 0.05 mM 2-mercaptoethanol. Human embryonic kidney (HEK) 293 and lung adenocarcinoma A549 cell lines were maintained in Dulbecco's modified Eagle's medium supplemented with 10% FBS (PAA Laboratories, Pasching, Austria). Dihydrofolate reductase-deficient Chinese hamster ovary (CHO) cells (CHO-DG44 cells) were maintained in RPMI-1640 supplemented with 10% FBS (PAA Laboratories).

Flow cytometric analysis. Daughter mouse ES cells isolated by the robot were cultured for 2–3 weeks to reach ~1×10^6 cells, and then harvested by trypsinization. The fluorescent intensities of ~2.0×10^4 cells from each clone were measured with a BD FACSCanto II flow cytometer (BD, Franklin Lakes, NJ, USA). Parental mouse ES and A549 cells were used as positive and negative controls, respectively. HyLDH/YK-1 cells treated with 1 μg ml^{-1} brefeldin A (BD) for 6 h were fixed in PBS containing 4% paraformaldehyde (PFA) at room temperature for 15 min, permeabilized with PBS containing 0.03% Triton X-100 at room temperature for 5 min and then collected by centrifugation (200 × *g*, 5 min). Cells were then incubated with 2 μg ml^{-1} FITC-conjugated anti-mouse $F(ab')_2$ rabbit $F(ab')_2$ (Rockland, Gilbertsville, PA, USA) in PBS at room temperature for 20 min, followed by FACS analysis. HEK 293 cells were used as a negative control.

Preparation of trapping molecules. For the cell-surface FIA, 1.65 nM Immunopure anti-mouse Fc goat polyclonal antibody (Thermo) was reacted with 66 μM DOPE-PEG2000-N-hydroxysuccinimide (NHS; NOF, Tokyo, Japan) in 100 μl sodium phosphate (10 mM, pH 7.6) and 250 mM NaCl at room temperature for 10 min. Free DOPE-PEG2000-NHS molecules were removed by ultrafiltration through 50 kDa cut-off membranes (Millipore, Billerica, MA, USA). Coupling of DOPE-PEG2000 to the antibody was confirmed by SDS-PAGE and Coomassie Brilliant Blue R-250 staining. To observe trapping molecules on the HyLHD/YK-1 cell surface, ~2.0×10^4 cells were combined with 100 μl serum-free RPMI-1640 medium containing 16 nM trapping molecules, incubated at 37°C for 10 min and then fixed with 4% PFA at room temperature for 20 min. Cells were washed with PBS twice, incubated in 100 μl PBS containing 400 ng Alexa 488-conjugated anti-goat IgG antibody (Invitrogen) at room temperature for 20 min, washed with PBS twice and then observed under a confocal laser-scanning microscope (FV-1000D; Olympus, Tokyo, Japan). To evaluate the cytotoxicity of the trapping molecule (DOPE-PEG2000-antibody) in HyLDH/YK-1 cells, ~1.25×10^5 cells in 2.5 ml culture medium were treated with the trapping molecule at 0.16–16 nM final concentration (as a protein concentration) and then maintained at 37°C with 5% CO_2 for 2 weeks. Cell viabilities were measured by trypan blue staining.

Cell-surface FIA. Approximately 5.0×10^4 HyLDH/YK-1 cells were combined with 100 μl serum-free RPMI-1640 medium containing 16 nM trapping molecules, incubated at 37°C for 10 min, mixed with 900 μl serum-free RPMI-1640 medium and then placed into microchambers by brief centrifugation. After addition of 100 μl FBS, cells on the microchamber array chip were incubated for 30 min in a CO_2 incubator to allow antibody secretion and then treated with 2 μg ml^{-1} FITC-labeled anti-mouse $F(ab')_2$ $F(ab')_2$ antibody to establish the cell-surface FIA. After incubation at room temperature for 10 min, cells were briefly washed twice with medium and then subjected to the automated single-cell analysis and isolation system.

Mouse IgG ELISA. Each well of a MaxiSorp 96-well plate (Thermo) was treated with 30 μl anti-mouse Fc antibody (10 ng μl^{-1}) at 4°C for 24 h, washed with 200 μl PBS containing 0.1% (vol/vol) Tween 20 (PBS-T) five times and then treated with 200 μl bovine serum albumin (5 μg μl^{-1}) in PBS at room temperature for 1 h. To measure the amount of secreted antibody from HyLDH/YK-1 cells isolated by the robot, each sample was added to an anti-mouse Fc-immobilized well, incubated at room temperature for 1 h and then washed with 200 μl PBS-T five times, followed by addition of 200 μl PBS-T containing 0.2 μl horse radish peroxidase-conjugated anti-mouse Ig (GE healthcare, Little Chalfont, Buckinghamshire). Plates were incubated at room temperature for 1 h and then washed with PBS-T five times, followed by addition of 100 μl 3,3′,5,5′-tetramethylbenzidine substrate (Thermo). The coloration reaction was performed at room temperature for 30 min, stopped by 100 μl H_2SO_4 (2 M) and then the absorbance at 450 nm was measured.

1. Caron, A. W. *et al.* Fluorescent labeling in semi-solid medium for selection of mammalian cells secreting high-levels of recombinant proteins. *BMC Biotechnol.* **9**, 42 (2009).
2. Huangfu, D. *et al.* Induction of pluripotent stem cells by defined factors is greatly improved by small-molecule compounds. *Nat. Biotechnol.* **26**, 795–797 (2008).
3. Kurimoto, K., Yabuta, Y., Ohinata, Y. & Saitou, M. Global single-cell cDNA amplification to provide a template for representative high-density oligonucleotide microarray analysis. *Nat. Protoc.* **2**, 739–752 (2007).
4. Wang, D. & Bodovitz, S. Single cell analysis: the new frontier in 'omics'. *Trends Biotechnol.* **28**, 281–290 (2010).
5. Narsinh, K. H. *et al.* Single cell transcriptional profiling reveals heterogeneity of human induced pluripotent stem cells. *J. Clin. Invest.* **121**, 1217–1221 (2011).
6. Toyooka, Y., Shimosato, D., Murakami, K., Takahashi, K. & Niwa, H. Identification and characterization of subpopulations in undifferentiated ES cell culture. *Development* **135**, 909–918 (2008).
7. Pilbrough, W., Munro, T. P. & Gray, P. Intraclonal protein expression heterogeneity in recombinant CHO cells. *PLoS One* **4**, e8432 (2009).
8. Yamamura, S. *et al.* Single-cell microarray for analyzing cellular response. *Anal. Chem.* **77**, 8050–8056 (2005).
9. Casanova, J. Stemness as a cell default state. *EMBO Rep.* **13**, 396–397 (2012).
10. Ohgushi, M. & Sasai, Y. Lonely death dance of human pluripotent stem cells: ROCKing between metastable cell states. *Trends Cell Biol.* **21**, 274–282 (2011).
11. Mendez, A. J. Monensin and brefeldin A inhibit high density lipoprotein-mediated cholesterol efflux from cholesterol-enriched cells. Implications for intracellular cholesterol transport. *J. Biol. Chem.* **270**, 5891–5900 (1995).
12. Serpieri, F. *et al.* Comparison of humanized IgG and FvFc anti-CD3 monoclonal antibodies expressed in CHO cells. *Mol. Biotechnol.* **45**, 218–225 (2010).
13. Choi, J. H. *et al.* Development and optimization of a process for automated recovery of single cells identified by microengraving. *Biotechnol. Prog.* **26**, 888–895 (2010).
14. Suzuki, M., Tanaka, H. & Iribe, Y. Detection and Collection System of Target Single Cell Based on pH and Oxygen Sensing. *J. Rob. Mechatron.* **22**, 639–643 (2010).
15. Kato, K. *et al.* Immobilized culture of nonadherent cells on an oleyl poly(ethylene glycol) ether-modified surface. *Biotechniques* **35**, 1014–1018, 1020–1021 (2003).
16. Kato, K., Itoh, C., Yasukouchi, T. & Nagamune, T. Rapid protein anchoring into the membranes of Mammalian cells using oleyl chain and poly(ethylene glycol) derivatives. *Biotechnol. Prog.* **20**, 897–904 (2004).
17. Frame, K. K. & Hu, W. S. The loss of antibody productivity in continuous culture of hybridoma cells. *Biotechnol. Bioeng.* **35**, 469–476 (1990).
18. Ben-David, U. & Benvenisty, N. The tumorigenicity of human embryonic and induced pluripotent stem cells. *Nat. Rev. Cancer* **11**, 268–277 (2011).
19. Fong, C. Y., Peh, G. S., Gauthaman, K. & Bongso, A. Separation of SSEA-4 and TRA-1-60 labelled undifferentiated human embryonic stem cells from a heterogeneous cell population using magnetic-activated cell sorting (MACS) and fluorescence-activated cell sorting (FACS). *Stem Cell Rev.* **5**, 72–80 (2009).
20. Tedder, T. F. & Isaacs, C. M. Isolation of cDNAs encoding the CD19 antigen of human and mouse B lymphocytes. A new member of the immunoglobulin superfamily. *J. Immunol.* **143**, 712–717 (1989).
21. Chilosi, M. *et al.* CD138/syndecan-1: a useful immunohistochemical marker of normal and neoplastic plasma cells on routine trephine bone marrow biopsies. *Mod. Pathol.* **12**, 1101–1106 (1999).
22. Harper, D. *et al.* In vitro and in vivo investigation of a novel monoclonal antibody to plasma cells (W5 mAb). *Xenotransplantation* **11**, 78–90 (2004).
23. Polson, A. G. *et al.* Expression pattern of the human FcRH/IRTA receptors in normal tissue and in B-chronic lymphocytic leukemia. *Int. Immunol.* **18**, 1363–1373 (2006).
24. Rosa, E. A., Lanza, S. R., Zanetti, C. R. & Pinto, A. R. Immunophenotyping of classic murine myeloma cell lines used for monoclonal antibody production. *Hybridoma (Larchmt)* **31**, 1–6 (2012).
25. Pantel, K. & Alix-Panabières, C. Circulating tumour cells in cancer patients: challenges and perspectives. *Trends Mol. Med.* **16**, 398–406 (2010).
26. Gupta, P. B. *et al.* Identification of selective inhibitors of cancer stem cells by high-throughput screening. *Cell* **138**, 645–659 (2009).
27. Kurokawa, M. *Advanced Micro & Nanosystems, LIGA and Its Applications* (Saile, V., Wallrabe, U., Tabata, O. & Korvink, J. G. eds) **7**, 323–335 (Wiley-VCH GmbH & Co. KGaA, 2009).

Acknowledgments

This study was supported in part by The Japan Science Society (H22 to N.Y.), Adaptable & Seamless Technology Transfer Program through Target-driven R&D (A-STEP) by the Japan Science and Technology Agency (JST) (AS231Z04687F to N.Y., AS2311699F to S.K.), Regional New Consortium Projects (H15 to S.K. and H17 to I.F., METI, Japan), the Program for Promotion of Basic and Applied Researches for Innovations in Bio-oriented Industry (H22-7, BRAIN to S.K., K. Tanizawa), the Health Labor Sciences Research Grant from the Ministry of Health Labor and Welfare (to SK), a Grant-in-Aid for Scientific Research (A) (21240052 to S.K.), the As One Corporation (to S.K., A. Kondo, I.F.), the Suzuken Memorial Foundation (10-013 to S.K.), the Nagase Science and Technology Foundation (H22-1 to S.K.) and the Canon Foundation (H22-1-7 to S.K.). We thank Satoshi Sugiyama and Ken-ichi Kimura (Furukawa) for technical support, and Masahiro Matsushita and Kenji Uemukai (As One) for advice.

Author contributions

N.Y. and S.K. conceived the project, designed and performed experiments, processed and analyzed data and wrote the manuscript. A. Kida, M.I., T.N., A.D.M. and K. Tatematsu

processed and analyzed data. X.J. and M.K. developed the robot and chips. I.N. and H.R.U. prepared mouse ES cell samples. A. Kondo, I.F., K. Tanizawa and S.K. coordinated the project.

Additional information

Supplementary information accompanies this paper at http://www.nature.com/scientificreports

Competing financial interests: The authors declare no competing financial interests.

How to cite this article: Yoshimoto, N. *et al.* An automated system for high-throughput single cell-based breeding. *Sci. Rep.* **3**, 1191; DOI:10.1038/srep01191 (2013).

analytical chemistry

Article

pubs.acs.org/ac

Cell Surface-Fluorescence Immunosorbent Assay for Real-Time Detection of Hybridomas with Efficient Antibody Secretion at the Single-Cell Level

Akiko Kida, Masumi Iijima, Tomoaki Niimi, Andrés D. Maturana, Nobuo Yoshimoto,* and Shun'ichi Kuroda*

Graduate School of Bioagricultural Sciences, Nagoya University, Nagoya 464-8601, Japan

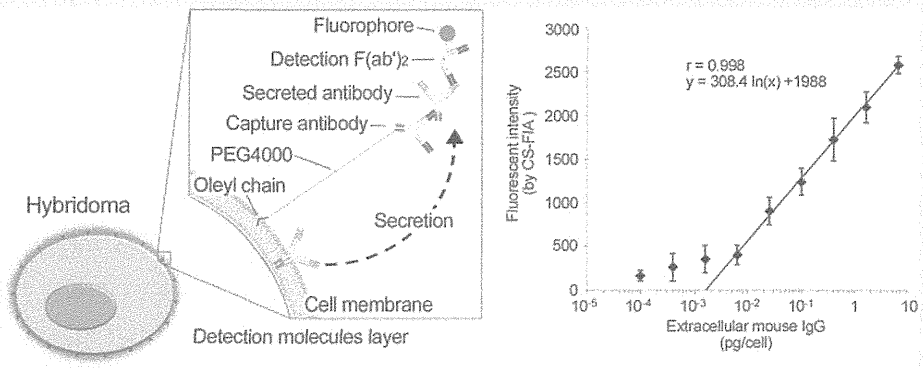

ABSTRACT: For establishing cells that secrete antibodies most efficiently (e.g., hybridomas, CHO (Chinese hamster ovary) cells), the screening and subsequent breeding of promising cells have been performed at the single-colony level, which requires several weeks to propagate a substantial number of cells by forming colonies from single cells for evaluation by the conventional assays. However, this screening process lacks high-throughput performance in time and colony numbers. Therefore, development of novel methods is expected to identify single cells secreting higher amounts of antibodies in real-time and in a nondestructive manner without colony formation. In this study, we prepared lipid-labeled antimouse IgG Fc antibodies (capture molecules) that were uniformly displayed on the surface of candidate cells. Secreted nascent antibodies were subsequently sandwiched between capture molecules and fluorescence-labeled antimouse IgG $F(ab')_2$ $F(ab')_2$ (detection molecules). This newly developed method is hereinafter referred to as a cell surface-fluorescence immunosorbent assay (CS-FIA). The fluorescence intensity of each cell was found to correlate well with the amount of sandwiched antibodies (from 6.25 fg/cell to 6.40 pg/cell). When about 4×10^3 cells of mouse hybridomas were subjected to CS-FIA, we isolated 28 hybridomas showing the highest fluorescence intensity within a day. Furthermore, after propagation of single cells to about 10^5 cells (after 2 weeks), 20 hybridomas were still able to secrete higher amounts (up to 7-fold) of antibodies than parental hybridomas. Our results demonstrate that CS-FIA is a powerful method for the single-cell-based establishment of cells that secrete most efficiently not only antibodies but also various biomolecules.

Mammalian cells, including hybridomas, Chinese hamster ovary (CHO) cells, and 293 cells, have been utilized to produce biomolecules (such as biomedicines), which have sustained not only biosciences but also bioindustries in the past 3 decades.[1−3] To establish such cells, it is important to identify cell clones stably and efficiently expressing materials of interest from a large number of candidates (screening process) and subsequently improve their productivity as much as possible (breeding process). During both processes, it is essential to routinely determine the productivity of individual cells. Conventionally, colonies derived from a single cell are propagated substantially and allowed to secret materials of interest into culture medium. Media are then subjected to immunoassays, such as 96- or 384-well immunoplate-based enzyme-linked immunosorbent assay (ELISA), for quantifying the amount of materials. However, this method is time-consuming and laborious. Specifically, when establishing hybridomas, candidate cells are split into single cells by a limiting dilution method,[4] allowed to grow for several weeks until the formation of colonies, and then subjected to immunoassays. To obtain cells with the most efficient secretion, several repetitions of the process and simultaneous culture of a large number of cells are both indispensable. Therefore, it is necessary to develop a new screening method that allows the identification of single cells secreting a higher amount of materials of interest in a real-time manner.

Typically, the coexpression of membrane protein CD20[5] and green fluorescence protein (GFP)[6] via the internal ribosomal

Received: October 22, 2012
Accepted: January 8, 2013
Published: January 8, 2013

entry site system enables candidate cells to be analyzed by fluorescence-activated cell sorting (FACS) to identify cells expressing higher amounts of CD20 and GFP. In the case of CHO dihydrofolate reductase gene (*dhfr*)-deficient cells, fluorescence-labeled methotrexate was used to identify CHO cells harboring higher copy numbers of *dhfr* gene.[7] However, the expression levels of products of interest do not always correlate with those of marker molecules, which prompted us to measure directly the secretion level of materials of interest at the single-cell level. Previously, Akselband et al.[8] reported the encapsulation of single cells into the gel microdrops containing biotinylated agarose, avidin, a biotinylated capture antibody, and a fluorescence-labeled detection antibody, through which secreted materials of interest were immobilized on the agarose matrix and detected as a fluorescence-labeled immunocomplex. The microdrops with the highest fluorescence intensity could then be selected by FACS (i.e., gel microdrop technology). The drawbacks of this method, however, include low encapsulation efficiency of cells (<15% of gel microdrops) and physical cell stress caused by a solid medium. In addition, Manz et al.[9] modified the cell surface chemically with biotin and then mixed cells with neutravidin, a biotinylated capture antibody, and a fluorescence-labeled detection antibody in a semisolid medium. Secreted materials of interest were immobilized as an immunocomplex in the vicinity of cells, and the cells with higher fluorescence intensity could be selected by FACS (i.e., matrix-based secretion assay). During these processes, the cells suffered from both physical stress caused by the semisolid medium and chemical stress by biotinylation. It was also noted that biotinylated cells tended to be agglutinated by neutravidin, thereby making the isolation of positive cells difficult at the single-cell level.

In the present study, we developed an easy-to-use and nondestructive method for identifying cells that secrete most efficiently at the single-cell level. First, we selected nontoxic lipid derivatives with higher cell adhesion activity. Second, capture antibodies were modified with selected lipid derivatives and mixed with candidate cells to display capture antibodies spontaneously and uniformly on the cell surface. Third, candidate cells were allowed to secrete materials of interest within a short period of time (~30 min) in normal medium and to form immunocomplexes with capture antibodies on the cell surface. Fourth, the fluorescence-labeled detection antibodies were added to the cells to exhibit fluorescence in a sandwich fluorescence immunosorbent assay (FIA), the intensity of which correlated well with the amount of secreted materials of interest. This screening method, designated as a cell surface-fluorescence immunosorbent assay (CS-FIA), could be applied to both the screening and subsequent breeding of various biomolecule-secreting mammalian cells.

EXPERIMENTAL SECTION

Cells. Hybridoma HyLDH·YK-1 (RCB0709) secreting anti-rabbit lactate dehydrogenase IgG1 was obtained from the RIKEN BioResource Center (Tsukuba, Japan). HyLDH·YK-1 cells were cultured in RPMI-1640 medium (Nacalai Tesque, Kyoto, Japan), supplemented with 10% (v/v) fetal bovine serum (FBS; Thermo, Waltham, MA), 100 μM nonessential amino acids (Invitrogen, Carlsbad, CA), and 50 μM 2-mercaptoethanol (Wako, Osaka, Japan), at 37 °C in 5% (v/v) CO_2 under humidified atmosphere. Dihydrofolate reductase-deficient CHO (CHO-DG44) cells (Invitrogen) were cultured in RPMI-1640 medium supplemented with 10% FBS (PAA Laboratories, Pasching, Austria).

Lipid-Labeled Antibodies. *N*-Hydroxysuccinimide-conjugated lipid derivative distearoylphosphatidylethanolamine (DSPE-NHS), DSPE-polyethylene glycol (PEG) 2000-NHS, DSPE-PEG3400-NHS, oleyl-PEG2000-NHS, oleyl-PEG4000-NHS, and dioleoylphosphatidylethanolamine (DOPE)-PEG2000-NHS were purchased from NOF (Tokyo, Japan). Goat-derived polyclonal antimouse IgG Fc antibodies (1.65 nmol; Immunopure, Thermo) were mixed with 66 nmol of NHS-conjugated lipid derivatives in 100 μL of sodium phosphate buffer (10 mM, pH 7.6) and NaCl (250 mM), incubated at room temperature for 10 min, and then concentrated using the Amicon Ultra-0.5 Centrifugal Filter Unit with Ultracel-50 Membrane (cutoff value, 50 kDa; Millipore, Billerica, MA) to obtain lipid-labeled antibodies. Antibody modifications with lipid derivatives were monitored by sodium dodecyl sulfate (SDS)-polyacrylamide gel electrophoresis (PAGE), followed by Coomassie Brilliant Blue (CBB) R-250 staining.

Quartz Crystal Microbalance. The amount of oleyl-PEG4000-labeled antimouse IgG antibodies bound to mouse IgG1 (1 mg/mL; Sigma-Aldrich Corp., St. Louis, MO) was determined by the quartz crystal microbalance (QCM) model Twin-Q (As One Corp., Osaka, Japan). The QCM sensor chip consists of a 9 mm-diameter disk made from an AT-cut 27-MHz quartz crystal with gold electrodes on each sides (diameter, 2.5 mm; area, 4.9 mm^2). A frequency change (ΔF) of 1 Hz corresponds to a weight change of 0.6 ng/cm^2. The temperature of the measuring bath (~600 μL) was maintained at 25 °C, with mixing at 600 rpm using a stirring tube. Samples were dissolved in 500 μL of phosphate-buffered saline (PBS; 137 mM NaCl, 10 mM Na_2HPO_4, 2 mM KH_2PO_4, pH 7.4). Triplicate measurements were made until a stable frequency (less than ±3 Hz) was observed for >1 min.

Cytotoxicity Test. HyLDH·YK-1 cells (approximately 2.0×10^4 cells/well) grown in 96-well plates were cultured for 24 h in the presence of either NHS-conjugated lipid derivatives or lipid-labeled antibodies (at final concentrations of 1.5, 15, and 150 nM). Cells were subsequently incubated for 2 h with 10 μL of the Cell Count Reagent SF (Nacalai Tesque) containing 2-(2-methoxy-4-nitrophenyl)-3-(4-nitrophenyl)-5-(2,4-disulfophenyl)-2H-tetrazolium (WST-8) and subjected to the measurement of absorbance at 450 nm by a Varioskan multiplate spectrophotometer (Thermo).

Cell Adhesion Assay. Dulbecco's PBS (D-PBS; 200 μL) containing 1% (w/v) bovine serum albumin (BSA) was added to each well of the Lab-Tek 8-well glass chamber slide system (Thermo) and incubated at room temperature for 36 h. After 2 washes with distilled water, 100 μM NHS-conjugated lipid derivatives in D-PBS (200 μL/well) was added and incubated at room temperature for 20 min. After washes with distilled water, HyLDH·YK-1 cells (about 2.0×10^5 cells) in 100 μL of D-PBS was added to each well and incubated at 37 °C for 5 min. After 3 washes with D-PBS, cells were observed under a FV1000D confocal laser scanning microscope (Olympus, Tokyo, Japan).

Cell Surface Display Assay. HyLDH·YK-1 cells (about 1.0×10^6 cells) were collected by brief centrifugation and incubated with 100 μL of 1 μM lipid-labeled antibodies at 37 °C for 10 min. After washes with D-PBS, cells were mixed with 4% (w/v) paraformaldehyde in D-PBS at room temperature for 20 min. After 2 washes with D-PBS, cells were mixed with 500 μL of Alexa 488-labeled donkey-derived antigoat IgG (H+L) (2.0 mg/mL; 1:1000; Invitrogen) and incubated at